Internship at Instituto Tecnológico de Aeronáutica (ITA)

Divisão de Engenharia Mecânica-Aeronáutica

On behalf of:

UNIVERSITEIT TWENTE.

Influence of Aileron Oscillation and Gap Size on Aerodynamic Control Derivatives

Author:

Timon Kruijk
s1007165

Supervisor at UT:
Prof. Dr. Ir. H.W.M. Hoeijmakers

Supervisors at ITA:
Prof. Roberto Gil Annes da Silva
Prof. Flávio José Silvestre

São José dos Campos, Brazil
Enschede, the Netherlands

February-May 2014

Preface

This internship project at Instituto Tecnológico de Aeronáutica in São José dos Campos, Brazil, has been carried out as part of my master programme Mechanical Engineering at the University of Twente in Enschede, The Netherlands. I would like to thank Prof. Dr. Ir. Harry Hoeijmakers in Enschede and Prof. Luiz Carlos Sandoval Góes in São José dos Campos for offering me the possibility to carry out my internship in Brazil. Furthermore, I would like to sincerely thank Prof. Roberto Gil Annes da Silva and Prof. Flávio José Silvestre at ITA for supervising me, for their excellent support during the preparations before departure and during my stay at ITA and for helping me with getting used to the daily life in Brazil. Also, I owe thanks to Prof. Maurício Morales and Prof. André Valdetaro Gomes Cavalieri at ITA for helping me when my supervisors were not able to do so. Furthermore, I would like to thank Mr. Eduardo Molina from Embraer, for helping me with the setup of the CFD simulations, for providing me with the necessary files and for helping me get acquainted with the software. Also, I would like to thank my friends and flatmates in São José dos Campos, who have made my stay a very enjoyable one. Finally, of these friends a special thank you is for Naira Cunha Costa, from ITA, who corrected the Portuguese version of the summary.

All of this would not have been possible without the financial support of the Twente Mobility Fund, on behalf of the University of Twente.

For me, this has been an unforgettable experience during which I have been able to catch a glimpse of the cultural diversity, linguistics and daily life in this immense country.

Summary - English

In the broad scope, this project is about the control of unmanned aircraft when applying a harmonic oscillation to the ailerons. It concerned a phenomenon that arises when oscillations are applied to flaps in airfoils. More specifically, it focused on defining a procedure to predict real-life values of two aerodynamical parameters concerning ailerons ($\partial c_l/\partial\beta$ and $\partial c_m/\partial\beta$) as a function of the aileron oscillation frequency (reduced frequency k) and the gap size between aileron and airfoil (ζ) using the theoretical background as the starting point. For simplicity, a 2D situation has been considered throughout the project. The theoretical background used here is the potential theory as defined by Theodorsen [2]. For simplicity, a flat plate is assumed as this is well described by the potential theory. The circulatory and non-circulatory parts of the flow have been considered separately in order to closely investigate the influence of each contribution. The lift force and moment are functions of three main variables: the heave, the rotation and the aileron rotation and the first and second derivative of each. As the case of an oscillating aileron is considered, the heave and rotation of the airfoil itself and their derivatives are assumed to be zero and are left out of the equation. The aileron motion is prescribed by a harmonic oscillation, which means that all relevant motions have been described.

For the model results, determined using MATLAB, a reference case has been defined which defines all other unknowns like atmospheric conditions, geometry and frequency range. This case refers to an aircraft flying at sea level with a Mach number of 0.2 and an aileron size of 20% of the airfoil chord. The investigated range of the reduced frequency is between 0 and 2. It turns out that for low frequencies, the circulatory part of the flow is the dominant contributor to both control derivatives and that for higher frequencies, the non-circulatory part of the flow becomes dominant. A sensitivity analysis has been performed to investigate the influence of several parameters. An empirical relation by Wright & Cooper [7] has been used to check the validity of the quasi-steady model when the main variable is the aileron location using zero oscillations. Due to a lack of time only the theory considering flap oscillations has been applied, gap flow has not been considered here.

Next, high-fidelity analyses using CFD have been performed for the same reference case. Here, both variables (k and ζ) have been considered. Considering the computation grid, there were two main problems. First of all, for each gap size a different mesh is needed as the geometry changes. This has been solved by using four different meshes, using 0, 2, 4 and 6% of the flap chord as the gap size. Finally, as an oscillation is applied to the aileron, the mesh is not constant over time. The mesh has been set up such that a harmonic oscillation can be applied to the aileron, specifying the maximum deflection, equilibrium position, oscillation frequency and hinge location in the configuration file. In each analysis, four oscillation periods have been calculated to get rid of any possible entrance effects, each oscillation period has been considered using at least 25 time steps. Analyses have been performed for each gap size using a reduced frequency of $k = 0.2$ and $k = 1$ and for 11 different frequencies using a gap size $\zeta = 2\%$ of the aileron chord. Varying frequency is easier in this case, as no new mesh is needed for each increment in frequency.

After performing the analyses, it turned out that when varying gap size the results were quite odd. One would have expected some kind of regression in the maximum value of c_l with increasing gap size as a larger gap implies a larger leakage flow, but this is not what followed from the results. Zooming in around the gap showed surprisingly that no gap flow was present at all, which highly questions the CFD results. The analyses in which only the frequency was varied produced more logical results, a similar progress for the control derivatives as a function of k was observed as in the theoretical model.

Finally, despite the sometimes questionable results, correction functions have been set up which correct the theoretical values of the control derivatives to the "real-life" values as simulated by CFD as a function of reduced frequency k and gap size ζ, respectively. Closely examining the flow field showed that the incompressibility assumption was valid and that that flow separation indeed occurred at the trailing edge, but the limitations of the potential theory and the quality of the CFD results limit and question the use of these specific results. However, when including theory about gap flow in the MATLAB model and using better practical results (from wind tunnel tests or from more accurate CFD calculations) the procedure in general might give a pretty good prediction of the desired parameters in future.

Resumo - Português

Este projeto, de maneira geral, trata da geração de forças e momentos aerodinâmicos quando uma oscilação harmônica é aplicada às superficies de controle. Mais especificamente, com foco na definição de um procedimento para prever valores reais de dois parâmetros aerodinâmicos ($\partial c_l/\partial\beta$ e $\partial c_m/\partial\beta$, as derivadas de controle) como uma função da frequência de oscilação do flape (a frequência reduzida k) e do espaço entre junções, fenda (ζ), utilizando o referencial teórico como ponto de partida. Para simplificar, uma situação 2D foi considerada ao longo do projeto cujo referencial teórico utilizado é a teoria do Potencial, conforme definido em Theodorsen. Uma placa plana é assumida como sendo melhor descrita pela teoria potencial, bem como as partes circulatórias e não circulatórias do fluxo foram considerados separadamente, a fim de investigar de perto a influência de ambas as contribuições. A força de sustentação e o momento são funções de três variáveis principais: o deslocamento vertical, a rotação, a rotação do aerofólio e suas primeiras e segundas derivadas. Como o caso de um aerofólio oscilante é considerado, o deslocamento vertical e a rotação estão assumidos como sendo zero, ficando fora da equação. O movimento do aileron é prescrito por uma oscilação harmônica, o que significa que todos os movimentos relevantes são conhecidos.

Para os resultados do modelo determinado usando o software MATLAB, um caso de referência foi criado definindo todas as outras incógnitas, como por exemplo: as condições atmosféricas, geometria e faixa de frequência. Este estudo de caso se refere a uma aeronave voando no nível do mar, com um número de Mach de 0,2 e um tamanho do aerofólio com 20% da corda do aerofólio. A faixa investigada da frequência reduzida está entre 0 e 2. Verificou-se que para as baixas frequências, a contribuição com circulação é dominante; e para as altas frequências, a contribuição sem circulação é dominante. Uma análise de sensibilidade foi realizada para investigar a influência dos outros parâmetros. Uma relação empírica determinada por Wright & Cooper [7] foi usada para verificar a validade do modelo quando a variável principal é a localização do aileron sem oscilações. Devido a falta de tempo, apenas a teoria considerando as oscilações do flap foi aplicada, o fluxo através do espaço entre as junções não foi considerado neste trabalho.

Em seguida, análises CFD foram realizadas para o mesmo caso de referência para simular a situação real. Neste caso, as duas variáveis (k e ζ) foram utilizadas. Considerando-se a malha de computação, existiam dois pontos de atenção principais: primeiramente, para cada tamanho de fenda é necessária uma malha diferente devido às alterações da geometria. Isto foi resolvido com a utilização de quatro malhas diferentes, utilizando-se os tamanhos das fendas de 0, 2, 4 e 6% da corda do aerofólio. Finalmente, como uma oscilação é aplicada para o aileron, a malha não é constante ao longo do tempo. A malha foi criada de tal forma que uma oscilação harmônica pode ser aplicada para o aileron, especificando a deflexão máxima, posição de equilíbrio, a frequência de oscilação e a localização da articulação no arquivo de configuração. Em seguida, para cada análise quatro períodos de oscilação foram calculados para evitar eventuais efeitos de entrada; cada período de oscilação foi considerado com pelo menos 25 intervalos de tempo. As análises foram realizadas para cada tamanho de abertura com uma frequência reduzida de $k = 0.2$ e $k = 1$ e para 11 frequências diferentes, utilizando como tamanho de abertura $\zeta = 2\%$ da corda do aileron. Neste caso, a variação da frequência é mais fácil, pois a mesma malha pode ser usada para todos os cálculos.

Depois da execução das análises, verificou-se que ao variar o tamanho da abertura os resultados apresentados estavam diferentes do esperado. Era esperado algum tipo de regressão no valor máximo de c_l com o aumento do tamanho de abertura ζ, pois uma abertura maior implica em um fluxo de fuga maior, no entanto, os resultados mostraram algo diferente. Quando o campo de fluxo é ampliado próximo a fenda, é mostrado que, surpreendentemente, não há fluxo de fuga presente em nenhum momento, o que questiona seriamente os resultados das análises CFD. As análises em que apenas a frequência foi variada produziram resultados mais lógicos. Um progresso similar ao das derivadas de controle como uma função de k foi observado no modelo teórico.

Finalmente, apesar dos resultados, por vezes questionáveis, funções de correção foram criadas para corrigir os valores teóricos das derivadas de controle para os valores "reais" simulados por CFD em função da frequência reduzida k e do tamanho da fenda ζ, respectivamente. Quando examinado, o campo de fluxo mostrou que o pressuposto de incompressibilidade é válido e que a separação do fluxo de fato ocorreu na borda de fuga. Porém, as limitações da teoria do potencial e a qualidade dos resultados de CFD limitam e questionam a aplicação neste caso específico. Entretanto, quando foi incluída a teoria sobre o fluxo através da fenda e com resultados reais mais certos (de experimentos em túnel de vento ou de cálculos CFD mais precisos) o procedimento, em geral, pode fornecer uma melhor previsão dos parâmetros desejados no futuro.

Contents

1 Introduction **1**

2 Literature study **3**
2.1 Aileron design . . . 3
2.2 Aerodynamics using potential theory . . . 3
2.2.1 Non-circulatory flow . . . 4
2.2.2 Circulatory flow . . . 5
2.2.3 Flap contribution . . . 9
2.3 Influence of flap oscillations . . . 10
2.4 Influence of gap flow . . . 10

3 Theoretical model **11**
3.1 Modeling background . . . 11
3.2 Reference case results . . . 12
3.3 Sensitivity analysis . . . 14

4 Numerical model in CFD **17**
4.1 Modeling background . . . 17
4.1.1 Meshing . . . 17
4.1.2 Analysis parameters . . . 18
4.2 Performed analyses . . . 19
4.3 Varying gap size . . . 19
4.3.1 CFD results . . . 19
4.3.2 Comparison with potential theory . . . 20
4.3.3 Gap flow observations . . . 21
4.4 Varying frequency . . . 22
4.4.1 CFD results . . . 22
4.4.2 Correction functions . . . 23

5 Conclusions and Recommendations **25**
5.1 General procedure . . . 25
5.2 Discussion . . . 25
5.2.1 Validity of the model . . . 26
5.2.2 Limitations of the used theory . . . 27
5.2.3 Discussion of the CFD results . . . 27
5.3 Recommendations . . . 28

List of Figures

2.1 Location of the aileron on the wing (a) and a cross section of the wing (b) . . . 3
2.2 Flat plate and the general outline of the Joukowsky transformation . . . 4
2.3 The application of the Kutta condition (from [4, p. 57]) . . . 6
2.4 An example of vorticity in the gap between airfoil and aileron using a discrete flap . . . 10

3.1 The control derivatives as function of k for the parameters stated in table 3.1 . . . 13
3.2 The control derivatives as function of k compared with Cooper's empirical relation . . . 13
3.3 Influence of the elastic axis location on the moment control derivative . . . 14
3.4 The progress of c_l in time for different values of β_0, using $k = 1$ . . . 15
3.5 $\partial c_l/\partial\beta$ as a function of the aileron location c . . . 15
3.6 $\partial c_m/\partial\beta$ as a function of the aileron location c . . . 16
3.7 $\partial c_l/\partial\beta$ as a function of the aileron location c, determined in two ways. . . . 16

4.1 The mesh seen from different zoom levels, for the case without gap, no flap deflection. . . . 17
4.2 The aileron shown in the extreme positions. . . . 18
4.3 Different gap sizes. . . . 18
4.4 The lift- and momentcoefficient for $k = 0.2$ . . . 20
4.5 The lift- and momentcoefficient for $k = 1$ . . . 20
4.6 Correction functions for the lift- and moment coefficient . . . 21
4.7 Distribution of C_p over and of M around the airfoil, for a 4% flap chord gap with maximum downward flap deflection. . . . 22
4.8 Correction factors for the lift- and moment coefficient . . . 23
4.9 Correction functions for both control derivatives . . . 23

5.1 Mach number distribution around the airfoil for zero gap, $k = 1$ and maximum downward aileron deflection. . . . 26
5.2 Mach number distribution around the trailing edge with $k = 1$ and maximum downward aileron deflection. 27
5.3 c_l for $k = 0.2$ and $\beta_0 = 0.1°$ . . . 28
5.4 c_l for $k = 0.2$, $\beta_0 = 3°$ and corrected for asymmetry. . . . 28

List of Tables

3.1 Parameters used in the reference calculation . . . 12

4.1 The performed analyses . . . 19

1 Introduction

This internship project has been carried out as part of my master programme Mechanical Engineering at the University of Twente (UT), The Netherlands. The general scope of this internship is to get acquainted with working on your own on a project in a real-life working or research environment. This three months' project can take place in a company, research institute or university, either within the Netherlands or abroad. I have been given the opportunity to perform my internship at the *Instituto Tecnológico de Aeronáutica* (ITA), an institute located in the city of São José dos Campos, São Paulo state, Brazil. This institute facilitates both aviation research and education at university level, with the support of the *Força Aérea Brasileira* (Brazilian Air Force), on behalf of the *Ministério da Defesa* (Ministry of Defense). ITA is located on a research campus called *Departamento de Ciência e Tecnologia Aeroespacial* (DCTA), which is the national military research centre for aviation and space flight of Brazil. ITA houses approximately 1,800 students and 180 academic staff members. Because the UT and ITA are partner universities, I had the opportunity to perform my internship at this institute as the effort needed to enter ITA was relatively little.

Scope of the research

In his doctorate research, Prof. Flávio J. Silvestre developed a methodology for modeling the dynamics of flexible aircraft by extending the rigid-body equations of motion with the aeroelastic dynamics, applied on slightly flexible aircraft in the incompressible flow regime [1]. During this research, Prof. Silvestre investigated several different maneuvers of these aircraft in order to improve the control of such aircraft. One of these maneuvers was to oscillate the control surfaces of the aircraft (elevator, ailerons, flaps and rudder) of the aircraft with a specified frequency to determine the aeroelastic response of the aircraft. During this research, Prof. Silvestre encountered a well-known phenomenon, namely that several aerodynamic parameters, like the derivatives of the lift and moment coefficients with respect to aileron angle, change when the oscillation frequency is increased. Quasi-steady semi-empirical formulas for the control derivatives were unable to predict the aerodynamic forces and moments generation in this case.

This project focused on investigating this well-known phenomenon using the theoretical background for a flat plate with an oscillating flap as defined by Theodorsen [2] and later on by simulating using CFD. The CFD analyses have been carried out using a thin, symmetrical airfoil and using different meshes that each have a different gap size between the airfoil and the aileron. The goal of the project is to define a procedure that determines correction functions for the lift and moment coefficient derivatives as a function of reduced frequency and gap size. The latter is considered such that significant nonlinear effects like gap flow which are not considered in the relatively simple potential theory are also accounted for. The used test section (2D) for the CFD analysis is a NACA0012 airfoil with three degrees of freedom (heave, rotation and flap rotation).

2 Literature study

2.1 Aileron design

Ailerons are structural elements of an airplane wing and they consist of two identical, symmetrically positioned flaps, located at the trailing edge of the outer portion of the wings, the farthest away from the fuselage. The primary function of the ailerons is to control the lateral movement of the aircraft and therefore the ailerons are usually used symmetrically: if one aileron points upward, the other one points downward. The design of the ailerons depends on many factors, like the aircraft structure, effectiveness, the required hinge moment to move the aileron, the aerodynamic and mass balances, the geometry of the flaps and the cost [3]. The location and geometry of the flaps are shown in figure 2.1, which is also shown in [3]. It should be noted that the symbols used in figure 2.1 are different from the symbols used throughout this report.

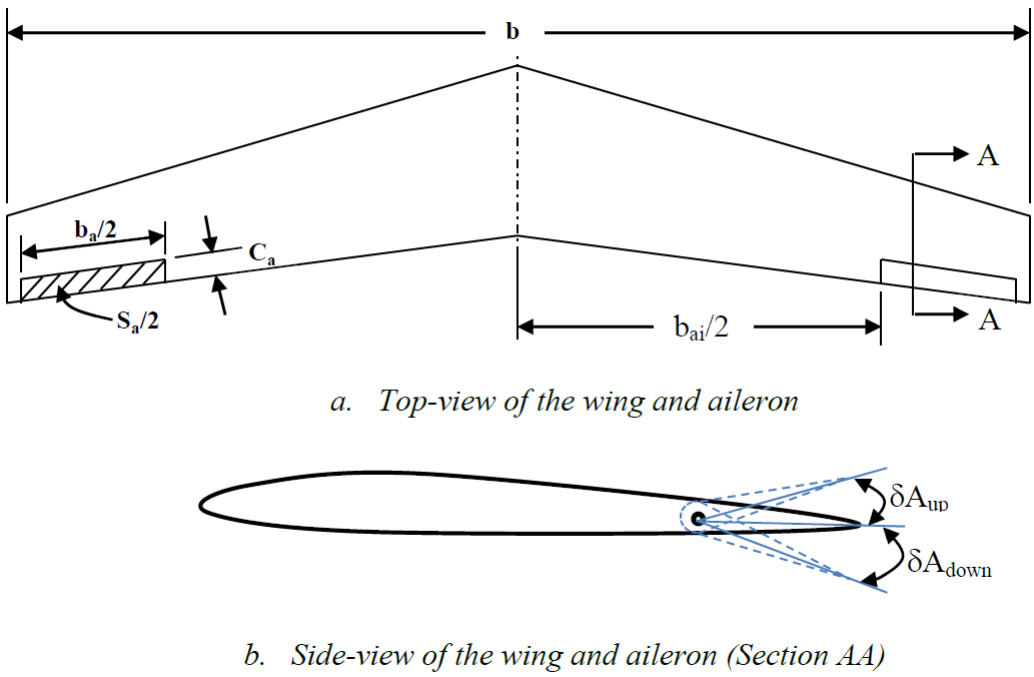

Figure 2.1: Location of the aileron on the wing (a) and a cross section of the wing (b)

2.2 Aerodynamics using potential theory

In order to investigate the flow around an airfoil (2D) with an aileron, like the one shown in figure 2.1b, a representing, simplified model will be build in MATLAB. The mathematical background of this model is potential flow which is a simplification of the real flow, making the mathematics of the problems much more bearable. In order to get to potential flow and a suitable model, this part of this research is based on the following assumptions:

- Unsteady flow
- Low velocities, so incompressible flow can be assumed ($M < 0.3$)
- Inviscid flow
- Irrotational flow, so there are no finite regions with finite vorticity, only infinitesimally small regions with infinite vorticity that have to be implemented in the flow field manually
- Conservative force field
- The Kutta-condition is needed to enforce flow separation at the trailing edge to prevent physically impossible flows

The unsteady aerodynamic forces are calculated using the linearized thin-airfoil theory. Theodorsen [2] calculated this using potential flow theory and he assumed that this unsteady flow consists of two components: non-circulatory flow and circulatory flow. The former is based on sources and sinks on the surface, the latter is based on trailing-edge vortices which are needed to satisfy the Kutta condition. For each component, the velocity potential can be determined separately. The derivation outlined here is a summary of the one shown in chapter 3.1 and 3.3 from [4] because the derivation as explained by Theodorsen himself (in [2]) is quite brief and lacks some explanation and is therefore hard to understand.

2.2.1 Non-circulatory flow

The non-circulatory flow can be visualized as a flat plate in uniform parallel horizontal flow, subjected to a heave h and an angular displacement α. Using conformal mapping, this can be transformed to a circle using Joukowski's transformation. At location (x_1, y_1) a source of strength 2ε is placed, at location $(x_1, -y_1)$ a sink of similar strength is placed. A schematic overview of this is shown in figure 2.2.

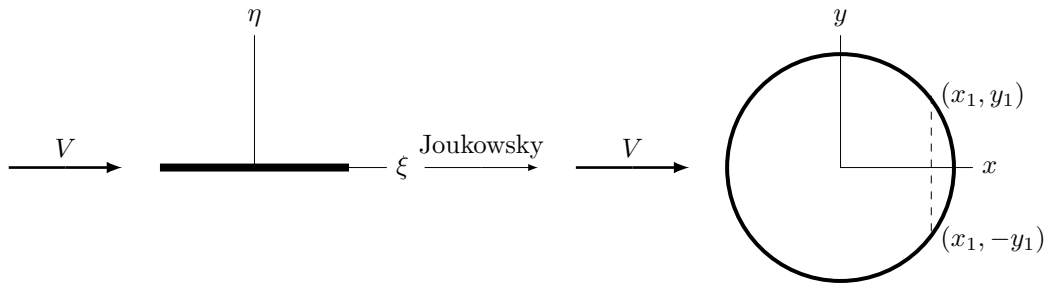

Figure 2.2: Flat plate and the general outline of the Joukowsky transformation

The velocity potential for a source of strength 2ε at position (x_1, y_1) and a sink of strength -2ε at position $(x_1, -y_1)$ is given by:

$$\begin{aligned}\phi &= \frac{\varepsilon}{2\pi}\ln\left[(x-x_1)^2+(y-y_1)^2\right] - \frac{\varepsilon}{2\pi}\ln\left[(x-x_1)^2+(y+y_1)^2\right] \\ &= \frac{\varepsilon}{2\pi}\ln\left[\frac{(x-x_1)^2+(y-y_1)^2}{(x-x_1)^2+(y+y_1)^2}\right]\end{aligned} \tag{2.1}$$

As a circular cylinder is considered and the radius b is defined as 1, $y = \sqrt{1-x^2}$, such that $y_1 = \sqrt{1-x_1^2}$ and therefore ϕ is a function of x and x_1 only. The strength of the sources and the sinks follow from the downward displacement of the airfoil, defined as:

$$z(x,t) = h + \alpha(x - ab) \tag{2.2}$$

where the product ab gives the location of the axis of rotation (the elastic axis) of the airfoil. The upwash can be defined from this, as the change in displacement going with the flow:

$$w_a(x,t) = -\left(\frac{\partial z}{\partial t} + V\frac{\partial z}{\partial x}\right) = -\left[\dot{h} + \dot{\alpha}(x-ab)\right] - V\alpha = \varepsilon \tag{2.3}$$

Inserting this in equation 2.1 gives:

$$\phi = \frac{-\left[\dot{h} + \dot{\alpha}(x-ab)\right] - V\alpha}{2\pi}\ln\left[\frac{(x-x_1)^2+(y-y_1)^2}{(x-x_1)^2+(y+y_1)^2}\right] \tag{2.4}$$

As the flow around this cylinder is built up from a row of infinitesimal sources and sinks on the domain for x_1, integrating part by part over $x_1 \in [-1, 1]$ results in the total velocity potential for the non-circulatory part of the flow:

$$\begin{aligned}\Phi_{NC} &= b\int_{-1}^{1}\phi_{NC}dx_1 \\ &= b\int_{-1}^{1}\frac{-\left[\dot{h} + \dot{\alpha}(x-ab)\right] - V\alpha}{2\pi}\ln\left[\frac{(x-x_1)^2+(y-y_1)^2}{(x-x_1)^2+(y+y_1)^2}\right]dx_1\end{aligned} \tag{2.5}$$

In order to solve this several standard integrals from [2] are needed. It should be noted that the integrals already include the aileron location c, but for now it is assumed that there is no aileron yet (and hence, $c = -1$). When still including c, the general standard integrals are:

$$\begin{aligned}
\int_c^1 \ln\left[\frac{(x-x_1)^2+(y-y_1)^2}{(x-x_1)^2+(y+y_1)^2}\right] dx_1 &= 2(x-c)\ln N - 2\sqrt{1-x^2}\cos^{-1}(c) \\
\int_c^1 \ln\left[\frac{(x-x_1)^2+(y-y_1)^2}{(x-x_1)^2+(y+y_1)^2}\right](x_1-c)dx_1 &= -\sqrt{1-c^2}\sqrt{1-x^2} - \cos^{-1}(c)(x-2c)\sqrt{1-x-^2} + (x-c)^2\ln N \\
\text{with } N &= \frac{1-cx-\sqrt{1-x^2}\sqrt{1-c^2}}{x-c} = \frac{1+x}{1+x} = 1 \ \ (\text{as } c=-1)
\end{aligned} \tag{2.6}$$

In [4], the integral in 2.5 is considered in three separate parts (for h, $\dot{\alpha}$ and α) and added afterwards. The evaluation of the integrals is therefore not considered here. Combining all terms yield the velocity potential for the non-circulatory part of the flow:

$$\Phi_{NC} = \left[V\alpha + \dot{h} + \dot{\alpha}b\left(\frac{x}{b} - a\right)\right] b\sqrt{1-x^2} \tag{2.7}$$

which is a fairly simple result.

The pressure can be obtained from Bernoulli, using:

$$\begin{aligned}
\Delta p &= -2\rho\left(\frac{\partial\Phi_{NC}}{\partial t} + \cancel{V\frac{\partial\Phi_{NC}}{\partial x}}\right) \\
&= -2\rho\dot{\Phi}_{NC}
\end{aligned} \tag{2.8}$$

In equation 2.8, the derivative of Φ with respect to x can be neglected, because the potential does not depend on y and is therefore independent of the vertical position. This also means that the pressure difference contribution by the derivative of Φ_{NC} with respect to x is zero, as the top and bottom contributions cancel each other. Therefore, this term can be left out from equation. Integrating the pressure distribution over x and multiplying with the semichord gives the downward force on the airfoil:

$$\begin{aligned}
F_{NC} &= b\int_{-1}^{1} \Delta p\, dx \\
&= -2\rho b\int_{-1}^{1} \dot{\Phi}_{NC} dx \\
&= -2\rho b^2\int_{-1}^{1} \sqrt{1-x^2}\left[V\dot{\alpha} + \ddot{h} + \ddot{\alpha}b\left(\frac{x}{2} - a\right)\right] dx \\
\rightarrow \text{Using integration by parts:} \quad &= -\pi\rho b^2\left(V\dot{\alpha} + \ddot{h} - ba\ddot{\alpha}\right)
\end{aligned} \tag{2.9}$$

Similarly, the contribution of the non-circular flow to the pitching moment can be determined:

$$\begin{aligned}
M_{NC} &= b\int_{-1}^{1} \Delta p(x-a)b dx \\
&= -2\rho b^2\int_{-1}^{1} \dot{\Phi}_{NC}(x-a)dx \\
&= \pi\rho b^2\left[V\dot{h} + ba\ddot{h} + V\dot{\alpha}^2 - b^2\left(\frac{1}{8} + a^2\right)\ddot{\alpha}\right]
\end{aligned} \tag{2.10}$$

2.2.2 Circulatory flow

The circulatory part of the flow is caused by the vortex distribution from the trailing edge to infinity, needed to fulfill the Kutta condition. Theodorsen employed the Kutta condition by a bound vortex distribution over the airfoil and a vortex distribution over the wake of the airfoil, as shown in figure 2.3.

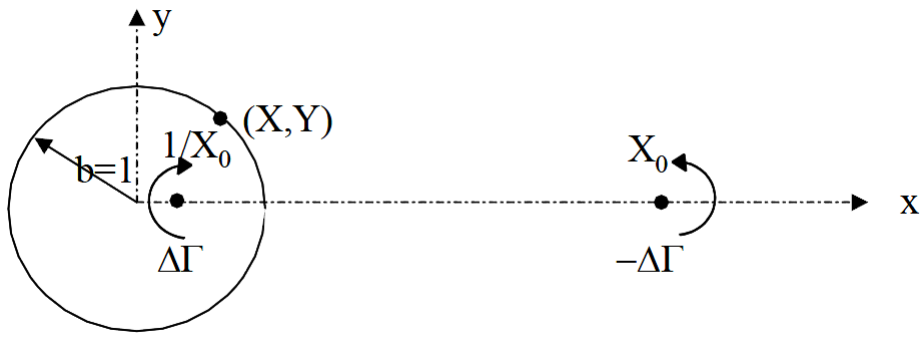

Figure 2.3: The application of the Kutta condition (from [4, p. 57])

According to Theodorsen [2], the velocity potential of the flow around a circle resulting from a vortex element $-\Delta\Gamma$ at $(X_0, 0)$ equals:

$$\begin{aligned}\Delta\phi_\Gamma &= \frac{\Delta\Gamma}{2\pi}\left[\tan^{-1}\frac{Y}{X-X_0} - \tan^{-1}\frac{Y}{X-\frac{1}{X_0}}\right] \\ &= \frac{\Delta\Gamma}{2\pi}\tan^{-1}\left(\frac{\left[X_0-\frac{1}{X_0}\right]Y}{X^2-\left[X_0+\frac{1}{X_0}\right]X+Y^2+1}\right)\end{aligned} \tag{2.11}$$

with (X, Y) the coordinates of the variables and X_0 the x-coordinate of the vortex element. Now defining the following:

$$\begin{aligned}X_0 + \frac{1}{X_0} &= 2x_0 \rightarrow X_0 = x_0 + \sqrt{x_0^2-1} \\ X &= x \\ Y &= \sqrt{1-x^2}\end{aligned} \tag{2.12}$$

and inserting these terms in equation 2.11 gives the following for the velocity potential contribution of the circulatory flow:

$$\begin{aligned}\Delta\phi_\Gamma &= -\frac{\Delta\Gamma}{2\pi}\tan^{-1}\left[\frac{2\sqrt{1-x^2}\sqrt{x_0^2-1}}{x^2-2xx_0+(1-x^2)+1}\right] \\ &= -\frac{\Delta\Gamma}{2\pi}\tan^{-1}\left[\frac{\sqrt{1-x^2}\sqrt{x_0^2-1}}{x^2-xx_0}\right]\end{aligned} \tag{2.13}$$

It should be noted here that the x-domain is similar as for the non-circulatory flow ($x \in [-1, 1]$) and that x_0 stretches from the trailing edge ($x = 1$) to infinity.

Again, Bernoulli can be applied to find the pressure difference. Here it should be noted that this time the velocity potential is time-independent and hence, the derivative of ϕ_Γ with respect to t yields zero. The derivative with respect to x consists of two components, one due to x and one due to x_0, the latter can be determined using the chain rule and the fact that $dx_0/dx = 1$. This means that the pressure difference is given by:

$$\Delta p_\Gamma = -2V\rho\left[\frac{\partial\Delta\phi_\Gamma}{\partial x} + \frac{\partial\Delta\phi_\Gamma}{\partial x_0}\frac{dx_0}{dx}\right] \tag{2.14}$$

with:

$$\begin{aligned}\frac{\partial\Delta\phi_\Gamma}{\partial x} &= -\frac{\Delta\Gamma}{2\pi}\sqrt{x_0^2-1}\frac{\partial}{\partial x}\left(\tan^{-1}\left[\frac{\sqrt{1-x^2}}{x^2-xx_0}\right]\right) \\ &= -\frac{\Delta\Gamma}{2\pi}\frac{\sqrt{x_0^2-1}}{\sqrt{1-x^2}}\frac{1}{x_0-x}\end{aligned} \tag{2.15}$$

and:

$$\begin{aligned}\frac{\partial \Delta\phi_\Gamma}{\partial x_0}\frac{dx_0}{dx} &= -\frac{\Delta\Gamma}{2\pi}\sqrt{1-x^2}\frac{\partial}{\partial x_0}\left(\tan^{-1}\left[\frac{\sqrt{x_0^2-1}}{x^2-xx_0}\right]\right) \\ &= -\frac{\Delta\Gamma}{2\pi}\frac{\sqrt{1-x^2}}{\sqrt{x_0^2-1}}\frac{1}{x_0-x}\end{aligned} \tag{2.16}$$

Inserting all in equation 2.14 and writing the two fractions in one term yields:

$$\Delta p_\Gamma = -\rho V\frac{\Delta\Gamma}{2\pi}\frac{x_0+x}{\sqrt{1-x^2}\sqrt{x_0^2-1}} \tag{2.17}$$

Like for the non-circulatory flow, this can be integrated over the chord to obtain the force. The difference here is that afterwards, the result needs to be integrated over x_0 in order to obtain the total force:

$$\begin{aligned}\Delta F_\Gamma &= b\int_{-1}^{1} -\rho V\frac{\Delta\Gamma}{2\pi}\frac{x_0+x}{\sqrt{1-x^2}\sqrt{x_0^2-1}}dx \\ &= -\rho V b\frac{x_0}{\sqrt{x_0^2-1}}\Delta\Gamma \\ \rightarrow F_\Gamma &= \int \Delta F_\Gamma = -\rho V b\int_1^\infty \frac{x_0}{\sqrt{x_0^2-1}}\gamma dx_0\end{aligned} \tag{2.18}$$

where $\Delta\Gamma = \gamma dx_0$. For the moment a similar procedure can be applied:

$$\begin{aligned}\Delta M_\Gamma &= b^2\int_{-1}^{1}\Delta p_\Gamma(x-a)dx \\ M_\Gamma &= \int \Delta M_\Gamma \\ &= \rho V b^2\int_1^\infty\left[\frac{1}{2}\sqrt{\frac{x_0+1}{x_0-1}} - \left(a+\frac{1}{2}\right)\frac{x_0}{\sqrt{x_0^2-1}}\right]\gamma dx\end{aligned} \tag{2.19}$$

In these expressions the vortex strength γ is still unknown, but it can be determined by applying the Kutta condition at the trailing edge and demanding that the solution is finite. Combining all terms of the velocity potential, and leaving Φ_Γ in the equation (as it has not been determined before) yields:

$$\Phi_{total} = \Phi_\Gamma + b\sqrt{1-x^2}\left(V\alpha + \dot{h} + \dot{\alpha}b\left(\frac{x}{2}-a\right)\right) \tag{2.20}$$

Now demanding that the solution at the trailing edge is finite gives:

$$\begin{aligned}\frac{\partial\Phi}{\partial x} &= finite \text{ at } x=1 \\ \left[\frac{\partial\Phi_\Gamma}{\partial x} - \frac{b}{\sqrt{1-x^2}}\left(V\alpha x + \dot{h}x + \dot{\alpha}bx\left(\frac{x}{2}-a\right) - \frac{1}{2}\dot{\alpha}b(1-x^2)\right)\right]_{x=1} &= 1 \\ \rightarrow \left[\sqrt{1-x^2}\frac{\partial\Phi_\Gamma}{\partial x}\right]_{x=1} &= V\alpha b + \dot{h}b + \dot{\alpha}b^2\left(\frac{1}{2}-a\right)\end{aligned} \tag{2.21}$$

Here it should be noted that Φ_Γ is unknown, but that there is an expression for $\Delta\Phi_\Gamma$ (equation 2.13). Differentiating this expression with respect to x gives:

$$\frac{\partial}{\partial x}\left(\Delta\phi_\Gamma\right) = \frac{\Delta\Gamma}{2\pi}\frac{\sqrt{x_0^2-1}}{\sqrt{1-x^2}}\frac{1}{x_0-x} \tag{2.22}$$

Inserting this in equation 2.21 and applying the integration over x_0 results in:

$$
\begin{aligned}
\left[\sqrt{1-x^2}\frac{\partial \Phi_\Gamma}{\partial x}\right]_{x=1} &= \int \frac{\Delta\Gamma}{2\pi}\frac{\sqrt{x_0^2-1}}{x_0-1} \\
&= \frac{b}{2\pi}\int_1^\infty \frac{\sqrt{x_0^2-1}}{x_0-1}\gamma dx_0 = V\alpha b + \dot{h}b + \dot{\alpha}b^2\left(\frac{1}{2}-a\right)
\end{aligned}
\tag{2.23}
$$

For convenience, this quantity is written as Q:

$$
\frac{b}{2\pi}\int_1^\infty \frac{\sqrt{x_0^2-1}}{x_0-1}\gamma dx_0 = V\alpha b + \dot{h}b + \dot{\alpha}b^2\left(\frac{1}{2}-a\right) \equiv Q \tag{2.24}
$$

Inserting this in the expressions for the force contribution of the circulatory flow gives:

$$
\begin{aligned}
F_\Gamma &= -\rho V b\int_1^\infty \frac{x_0}{\sqrt{x_0^2-1}}\gamma dx_0 \\
&= -2\pi\rho V b Q\frac{\int_1^\infty \frac{x_0}{\sqrt{x_0^2-1}}\gamma dx_0}{\int_1^\infty \frac{\sqrt{x_0^2-1}}{x_0-1}\gamma dx_0} \\
&= -2\pi\rho V b Q\frac{\int_1^\infty \frac{x_0}{\sqrt{x_0^2-1}}\gamma dx_0}{\int_1^\infty \frac{\sqrt{x_0+1}}{\sqrt{x_0-1}}\gamma dx_0} \\
&= -2\pi\rho V b Q C
\end{aligned}
\tag{2.25}
$$

with:

$$
C = \frac{\int_1^\infty \frac{x_0}{\sqrt{x_0^2-1}}\gamma dx_0}{\int_1^\infty \frac{\sqrt{x_0+1}}{\sqrt{x_0-1}}\gamma dx_0} \tag{2.26}
$$

which is defined as the *Theodorsen function*. This expression can also be inserted in the momentum equation, namely:

$$
\begin{aligned}
M_\Gamma &= \rho V b^2\int_1^\infty \left[\frac{1}{2}\sqrt{\frac{x_0+1}{x_0-1}} - \left(a+\frac{1}{2}\right)\frac{x_0}{\sqrt{x_0^2-1}}\right]\gamma dx \\
&= -2\pi\rho V b^2 Q\left[\frac{1}{2} - C\left(a+\frac{1}{2}\right)\right]
\end{aligned}
\tag{2.27}
$$

Assuming that the airfoil oscillates harmonically with a reduced frequency k, Theodorsen stated that:

$$
\begin{aligned}
C &= \frac{\int_1^\infty \frac{x_0}{\sqrt{x_0^2-1}}e^{-ikx_0}dx_0}{\int_1^\infty \frac{\sqrt{x_0+1}}{\sqrt{x_0-1}}e^{-ikx_0}dx_0} \\
&= F(k) + iG(k) = C(k)
\end{aligned}
\tag{2.28}
$$

such that it can be seen that the Theordorsen function is a function of the reduced frequency *only*. A further analysis of the Theodorsen function is left out here, it is only noted that it can be expressed in terms of Bessel functions (exact) or in terms of an algebraic approximation (not exact).

Finally, the circulatory and non-circulatory contributions of the force and moment are combined to end up with the final expressions for the lift and moment for an oscillating, rigid airfoil:

$$
\begin{aligned}
F &= F_\Gamma + F_{NC} = -\pi\rho b^2\left[\ddot{h} + V\dot{\alpha} - ba\ddot{\alpha}\right] - 2\pi\rho V b Q C(k) \\
M &= \pi\rho b^2\left[ba\ddot{h} - vb\left(\frac{1}{2}-a\right)\dot{\alpha} - b^2\left(\frac{1}{8}+a^2\right)\ddot{\alpha}\right] + 2\pi\rho V b^2\left(a+\frac{1}{2}\right)QC(k) \\
&\text{with } Q = V\alpha + \dot{h} + \dot{\alpha}b\left(\frac{1}{2}-a\right)
\end{aligned}
\tag{2.29}
$$

2.2.3 Flap contribution

If a flap is added, with an angle β with respect to the chord line and located at a distance bc from the midchord, the airfoil displacement becomes:

$$z = h + \alpha(x - ab) + \beta(x - bc)U(x - bc) \tag{2.30}$$

where $U(x - bc)$ is the unit step function. Like in the previous sections, the upwash, velocity potential, pressure distribution, force and moment can be determined. It should be noted here that the N-function, as shown in equation 2.6 is no longer equal to one, but remains dependent of c in order to preserve generality. Using this procedure, the force, moment and hinge-moment can be determined. The derivation of this is not presented here, but the interested reader is directed to [2] and [4]. The resulting equations for the force, moment and hinge moment, with the aileron included, are:

$$F = -\pi\rho b^2 \left[\ddot{h} + V\dot{\alpha} - ba\ddot{\alpha} - \frac{V}{\pi}T_4\dot{\beta} - \frac{b}{\pi}T_1\ddot{\beta}\right] - 2\pi\rho VbQC(k) \tag{2.31}$$

$$\begin{aligned} M =& \pi\rho b^2 \left[ba\ddot{h} - Vb\left(\frac{1}{2} - a\right)\dot{\alpha} - b^2\left(\frac{1}{8} + a^2\right)\ddot{\alpha} - \frac{V^2}{\pi}(T_4 + T_{10})\beta + \frac{Vb}{\pi}\left\{-T_1 + T_8 + (c - a)T_4 - \frac{1}{2}T_{11}\right\}\dot{\beta}\right. \\ &\left. + \frac{b^2}{\pi}\left\{T_7 + (c - a)T_1\right\}\ddot{\beta}\right] + 2\pi\rho Vb^2\left(a + \frac{1}{2}\right)QC(k) \end{aligned} \tag{2.32}$$

$$\begin{aligned} M_\beta =& \pi\rho b^2 \left[\frac{b}{\pi}T_1\ddot{h} + \frac{Vb}{\pi}\left\{2T_9 + T_1 - \left(a - \frac{1}{2}\right)T_4\right\}\dot{\alpha} - \frac{2b^2}{\pi}T_{13}\ddot{\alpha} - \left(\frac{V}{\pi}\right)^2(T_5 - T_4T_{10})\beta. + \frac{Vb}{2\pi^2}T_4T_{11}\dot{\beta} + \left(\frac{b}{\pi}\right)^2 T_3\ddot{\beta}\right] \\ &- \rho Vb^2T_{12}QC(k) \end{aligned} \tag{2.33}$$

with:

$$Q = V\alpha + \dot{h} + \dot{\alpha}b\left(\frac{1}{2} - a\right) + \frac{V}{\pi}T_{10}\beta + \frac{b}{2\pi}T_{11}\dot{\beta} \tag{2.34}$$

These functions contain several T-functions, which are defined in [4] and all of which are functions of c only. With a prescribed motion of the aileron, these equations can be applied in a mathematical model in two ways. The first way is if the heave and the rotation are released, only restricted by for example translational and rotational springs and dampers, the motion of the airfoil can be computed in time. In this case, it is assumed that the aileron oscillation is controlled perfectly and hence, the hinge moment from equation 2.33 can be neglected. Using this and using the Lagrange's equations, the equations of motion of the airfoil can be defined. The procedure of getting to this form is left out here, but it is shown briefly in sections 3.2 and 3.3 of [4]. Hence:

$$\begin{bmatrix} m & mx_\theta \\ mx_\theta & mr_\theta^2 \end{bmatrix} \begin{Bmatrix} \ddot{h} \\ \ddot{\alpha} \end{Bmatrix} + \begin{bmatrix} K_h & 0 \\ 0 & K_T \end{bmatrix} \begin{Bmatrix} h \\ \alpha \end{Bmatrix} = \begin{Bmatrix} F \\ M \end{Bmatrix} \tag{2.35}$$

In this equation, the force and moment contributions are given by equations 2.31 and 2.32, which include the (prescribed) motion of the aileron. This means that equation 2.35 is a system of two second-order ordinary differential equations (ODE's). This can be rewritten to four first order ODE's which can be integrated in time using standard tools in MATLAB. To check if such a model produces physically possible results it, could be verified using standard airfoil dynamics.

The second way to use this model is by not only prescribing the aileron motion, but also the heave and the rotation, as if the airfoil were located in e.g. a wind tunnel and fully controlled. This way the force, moment and hinge moment can be determined for a defined set of aileron oscillation frequencies and with that, the desired control derivatives can also be calculated. Here it should be noted that choosing any value for the heave does not influence the calculations, which is expected as the heave is only a relative quantity. A model of this kind can be verified using e.g. zero excitation of the aileron and a constant value for the angle of attack. In that case the lift coefficient from the model should equal the lift coefficient determined from the flat plate theory.

2.3 Influence of flap oscillations

The influence on the lift and moment coefficients of a harmonically oscillating airfoil with a harmonically oscillating flap (aileron) has been investigated by Krzysiak and Narkiewicz [5], hereby comparing a theoretical model and wind tunnel tests. Here it turned out that the correlation between the wind tunnel tests and the theoretical model is adequate and produce similar results. Their primary observation was that the plots of the lift and moment coefficients versus the angle of attack have the form of dual loops, whose shape depend greatly on the phase-shift angle between the motion of the airfoil and flap. This is a logical explanation, as the maximum lift is obtained when the airfoil and flap angle increase simultaneously and minimum lift is obtained when they rotate in anti-phase.

In case of a controlled aileron and a "free" airfoil the expected result is that because of the prescribed harmonic motion of the aileron, the airfoil will also rotate with an equal frequency, but some phase-delay is expected. From the results obtained by Krzysiak and Narkiewicz it turns out that the progress of the phase delay should be considered carefully, as this alters the resulting lift and moment coefficients quite significantly. If the phase delay is constant, as expected, it should be easy to calculate the control derivatives accurately as it has no further influence on the respective coefficients.

2.4 Influence of gap flow

In a theoretical model which assumes steady flow, it is assumed that the connection of the aileron to the airfoil is ideal and that no additional effects occur due to this connection. In reality, there are several significant effects due to a non-ideal connection, mainly caused by the gap between the airfoil and the aileron. This gap is needed to allow the aileron to rotate relative to the airfoil. However, because of the pressure difference between the upper and lower surface of the airfoil and because of the sudden change in airfoil geometry, the lift decreases and the drag increases if an aileron is used due to the presence of leakage flow and surface discontinuities.

Liggett and Smith [6] investigated these phenomena using CFD, more specifically the Reynolds-Averaged Navier-Stokes equations (RANS) and the Large-Eddy-Simulation (LES) turbulence technique, and they compared the results with experimental data to check the validity. In their research, they investigated two different flap situations: an integrated flap and a discrete flap. In the former case the shape of the connection ensures a more continuous geometry in the connection, in the latter case this connection is quite discrete such that the gap is larger and hence, the effects of the gap are expected to be much more significant. An example of a discrete flap geometry is shown below in figure 2.4.

The most important conclusions that Liggett and Smith draw are that the difference between the contoured and the non-contoured gaps are significantly large. The lift-to-drag ratio is 40% lower in case a discrete flap was used, at low angles of attack. The lift is higher in case a contoured gap is used, as the gap flow is much smaller. Also, due to flow separation, regions of high vorticity emerge in the gap region, which influence the main flow around the airfoil. An example of this is shown in figure 2.4, which is figure 4a from [6]. The direction of the flow through the gap turns out to be dominated by the flap direction relative to the airfoil. In stall conditions, the flow direction is always upward as stall occurs in maximum lift conditions, such that there is a maximum pressure difference between the upper and lower surface of the airfoil. The final conclusion that Liggett and Smith state is that even though gap flows delay stall, due to the loss in lift, discrete flaps are not recommended for application in practice. They discourage this due to the large performance losses which primarily occur at low angles of attack. In cruise flight, airplanes usually fly at low angles of attack, which is one of the main reasons why flap geometry is so important here.

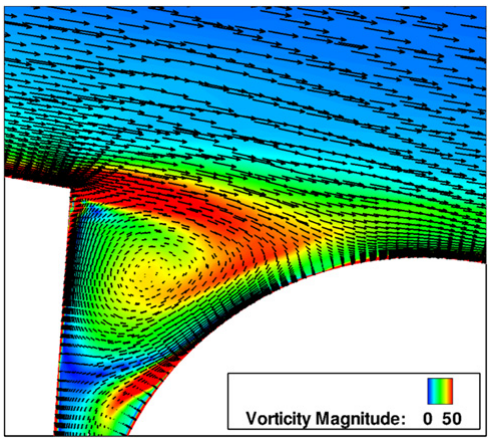

Figure 2.4: An example of vorticity in the gap between airfoil and aileron using a discrete flap

3 Theoretical model

3.1 Modeling background

As stated in the end of section 2.2.3, the found theory can be applied in a mathematical model in two different ways. The easiest of the two presented ways is by prescribing the motions of all three degrees of freedom: the heave, the rotation and the aileron rotation, which will be applied here. As stated in the section 2.2.3, the heave does not influence the resulting force and moments, as the orientation of the airfoil relative to the flow is not changed. Assuming that the vertical position of the airfoil is fixed and that only a constant angle of attack is prescribed, equations 2.31 and 2.32 reduce to:

$$F = -\pi\rho b^2 \left[-\frac{V}{\pi} T_4 \dot{\beta} - \frac{b}{\pi} T_1 \ddot{\beta} \right] - 2\pi\rho V b Q C(k) \tag{3.1}$$

$$\begin{aligned} M =& \pi\rho b^2 \left[-\frac{V^2}{\pi}(T_4 + T_{10})\beta + \frac{Vb}{\pi}\left\{ -T_1 + T_8 + (c-a)T_4 - \frac{1}{2}T_{11} \right\} \dot{\beta} \right. \\ &\left. + \frac{b^2}{\pi}\left\{ T_7 + (c-a)T_1 \right\} \ddot{\beta} \right] + 2\pi\rho V b^2 \left(a + \frac{1}{2} \right) Q C(k) \end{aligned} \tag{3.2}$$

with:

$$Q = V\alpha + \frac{V}{\pi} T_{10}\beta + \frac{b}{2\pi} T_{11}\dot{\beta} \tag{3.3}$$

It should be noted that both the force and the moment are complex numbers, because of the Theodorsen function and hence, they both have an amplitude and a phase. In order to be able to properly compare the contributions of the circulatory and the non-circulatory part of the flow, initially only the real part is considered. This way it is possible to visualize which contribution has the most effect for a given frequency. Furthermore, it should be noted that the force as presented in equation 3.1 is defined with the positive direction downward. Therefore the lift force is given by the negative of equation 3.1. Keeping this in mind and splitting the circulatory and non-circulatory contributions gives:

$$l = l_\Gamma + l_{NC} \tag{3.4}$$

with:

$$l_\Gamma = 2\pi\rho_\infty V_\infty b C(k) \left[V_\infty \alpha + \frac{V_\infty}{\pi} T_{10}\beta + \frac{b}{2\pi} T_{11}\dot{\beta} \right] \tag{3.5}$$

$$l_{NC} = \pi\rho_\infty b^2 \left[-\frac{V_\infty}{\pi} T_4 \dot{\beta} - \frac{b}{\pi} T_1 \ddot{\beta} \right] \tag{3.6}$$

and:

$$m = m_\Gamma + m_{NC} \tag{3.7}$$

with:

$$m_\Gamma = 2\pi\rho_\infty V_\infty b^2 \left(a + \frac{1}{2} \right) C(k) \left[V_\infty \alpha + \frac{V_\infty}{\pi} T_{10}\beta + \frac{b}{2\pi} T_{11}\dot{\beta} \right] \tag{3.8}$$

$$m_{NC} = \pi\rho_\infty b^2 \left[-\frac{V_\infty^2}{\pi}(T_4 + T_{10})\beta + \frac{V_\infty b}{\pi}\left\{ -T_1 + T_8 + (c-a)T_4 - \frac{1}{2}T_{11} \right\} \dot{\beta} + \frac{b^2}{\pi}\left\{ T_7 + (c-a)T_1 \right\} \ddot{\beta} \right] \tag{3.9}$$

Please note that *small* letters have been used to indicate these quantities, as they are given per unit span. Also, the subscript "∞" has been added to the density and velocity to indicate the free stream conditions. The lift and moment coefficients can be determined using the standard relations:

$$c_l = \frac{l}{qc} = \frac{l_\Gamma + l_{NC}}{\frac{1}{2}\rho_\infty V_\infty^2 c} \tag{3.10}$$

$$c_m = \frac{m}{qc^2} = \frac{m_\Gamma + m_{NC}}{\frac{1}{2}\rho_\infty V_\infty^2 c^2} \tag{3.11}$$

The MATLAB model has been programmed such that a certain range has to be given for the reduced frequency for which the control derivatives are desired. Using this, the angular frequency of the harmonic motion of the aileron is determined using parameters from a reference case which will be defined below. Applying everything yields the lift force and moment in time, with which the lift and moment coefficients are computed in time for one aileron oscillation. The change of β in time is also known and hence, the control derivatives can be computed. As only the real part is considered, both the lift and moment coefficients the contributions of the circulatory and non-circulatory flows to the control derivatives can be considered separately and they can be added for the total value.

As a final check, the found values for the case of *no* flap oscillation can be checked with the empirical relation defined by Wright & Cooper [7], who give a relation for the control derivative with respect to the angle of attack, control surface size and the control derivatives with respect to the angle of the control surface:

$$\frac{\partial c_l}{\partial \beta} = \frac{\frac{\partial c_l}{\partial \alpha}}{\pi}\left(\arccos(1-2E) + 2\sqrt{E(1-E)}\right) \tag{3.12}$$

$$\frac{\partial c_m}{\partial \beta} = -\frac{\frac{\partial c_l}{\partial \alpha}}{\pi}(1-E)\sqrt{E(1-E)} \tag{3.13}$$

where E is the ratio between the chord of the control surface and the airfoil chord.

3.2 Reference case results

The main case which is considered is the case in which the aircraft is flying at low altitude at a velocity for which incompressibility can still be assumed and hence, $M < 0.3$. In this situation the control surface consists of the last 20% of the airfoil. An overview of the quantities used in this reference calculation is presented in table 3.1.

Parameter	Symbol	Quantity
free stream density	ρ_∞	1.2886 kg/m^2
semi-chord	b	1 m
aileron location	c	0.6
elastic axis location	a	-0.2
Mach number	M	0.2
temperature	T	273.15 K
gas constant	R	287.87 J/kgK
max. aileron deflection	β_0	3°
airfoil angle of attack	α	0°
reduced frequency	k	[0.01,2]

Table 3.1: Parameters used in the reference calculation

From the specified values considering the geometry it can be seen that the ratio E equals 0.2. In combination with the standard theoretical value of the lift slope (2π), this can be applied to equations 3.12 and 3.13 to compute the theoretical value of the control derivatives in case of no oscillation, which can be used later on to validate the model:

$$\frac{\partial c_l}{\partial \beta} = \frac{2\pi}{\pi}\left(\arccos(1-2\cdot 0.2) + 2\sqrt{0.2\cdot(1-0.2)}\right) = 3.4546 \tag{3.14}$$

$$\frac{\partial c_m}{\partial \beta} = -\frac{2\pi}{\pi}(1-0.2)\sqrt{0.2(1-0.2)} = -0.64 \tag{3.15}$$

These values should equal the values of the non-circulatory contribution of the control derivatives that follow from the model in case $k = 0$. It should be noted that only the non-circulatory part should be considered here, as Q from equation 3.3 equals zero due to the absence of flap motion.

In the figures in 3.1 the control derivatives ($\partial c_l/\partial\beta$ and $\partial c_m/\partial\beta$) are shown as a function of the reduced frequency. All control derivatives have been shown as a total and with the circulatory and non-circulatory part of the flow split up.

From figure 3.1a it can be seen that for low frequencies the circulatory part of the contribution is the largest contributor to the control derivative. For high frequencies, the non-circulatory part is dominant. This may sound conflicting, but it can be explained using equations 3.4 to 3.6. For low frequencies, the derivatives of β are negligible compared to the

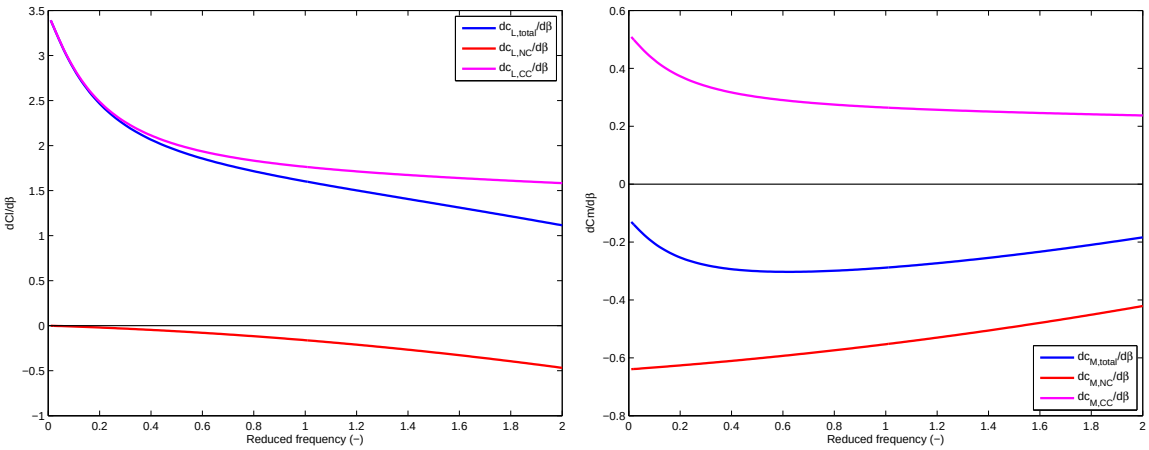

(a) $\partial c_l/\partial\beta$ (b) $\partial c_m/\partial\beta$

Figure 3.1: The control derivatives as function of k for the parameters stated in table 3.1

value of β itself. The real part of the Theodorsen function equals one for $k = 0$ and it decreases asymptotically to 0.5 and hence, for low values of k the circulatory part is the dominant contributor. As k increases, $\dot{\beta}$ increases linearly and $\ddot{\beta}$ increases quadratically and becomes the dominant term. If the calculation would be performed to (unrealistically) high values of k this behaviour would be even clearer. Similar behaviour is visible for the derivative of the moment coefficient as just like for the derivative of the lift coefficient, the non-circulatory contribution contains the second time derivative of β, whereas the highest derivative of β in the circulatory contribution is only $\dot{\beta}$. The only difference here is that in the limit case for $k \to \infty$ the value for $\partial c_l/\partial\beta$ diverges to $-\infty$, while the value for $\partial c_m/\partial\beta$ diverges to $+\infty$.

As a check, returning to the results in equations 3.14 and 3.15 and looking at both figures in 3.1 it indeed seems that the values for low frequency oscillations correspond with each other. Reconsulting the model for extremely low reduced frequencies, it turns out that the non-circulatory contribution for the lift control derivative for $k = 1 \cdot 10^{-5}$ equals 3.4545, which is significantly close to the value determined in equation 3.14, from the empirical relation from [7]. In case of the moment control derivative, the model yields -0.6400 for the same value of k, which corresponds with the value determined in 3.15, which is 0.64. Finally, it should be noted that the circulatory part in figure 3.1b does not yield zero for low frequencies, in contrary to what was stated before. This is due to the fact that even for very low frequency, the derivative of the excitation ($\dot{\beta}$) still has a nonzero value. This is not incorrect, but merely shows why only the non-circulatory part should be considered in case of $\partial c_m/\partial\beta$. The control derivatives as determined by Cooper can be compared to the values as determined by Theodorsen. This is shown in figure 3.2, where the control derivatives are shown. The total absolute value in case of $\partial c_l/\partial\beta$ and the *negative* of the absolute value of the non-circulatory part in case of $\partial c_m/\partial\beta$ have been used. In both cases, the sign of the control derivative should equal the sign of the real part of it, which is negative in the latter case. The magenta line in each figure represents a correction factor between the potential theory and Cooper's relation. This correction factor is indeed 1 for $k = 0$ and lower than 1 for $k > 0$ in both cases. This is expected as Cooper's relation is independent of k and the control derivatives decrease with increasing k, as shown in figure 3.1.

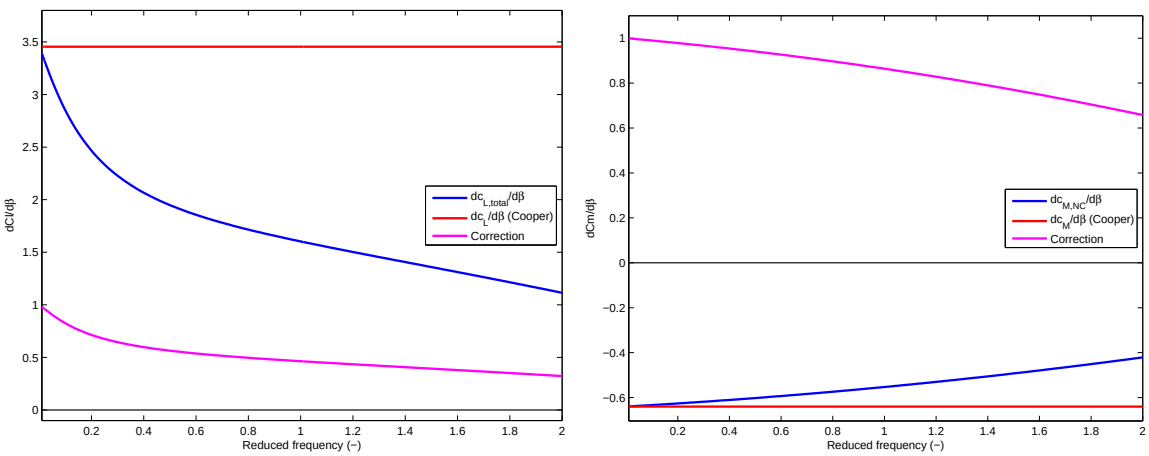

(a) $\partial c_l/\partial\beta$ (b) $\partial c_m/\partial\beta$

Figure 3.2: The control derivatives as function of k compared with Cooper's empirical relation

3.3 Sensitivity analysis

The parameters defined for the reference case in table 3.1 can be altered one by one to investigate the influence and sensitivity of each of the parameters.

Density

The density used in the standard case applies to the case when the flow is considered to be at a low altitude, such that $\rho = 1.2886\ kg/m^3$. In case the aircraft is flying at higher altitudes, the density decreases. However, from the used equations it can immediately be seen that this has no influence. In both terms of the expressions for the lift and the moment the density appears in the numerator once. In the equations for the respective coefficients the density appears in the denominator once such that these terms cancel each other. Hence, it can be concluded that altering the density has no influence on the change of the control derivatives with increasing oscillation frequency.

Elastic axis location

The location of the elastic axis is only important in case of the moment coefficient derivative, as the moment is determined around this point. In the reference analysis the elastic axis was located at 40% of the chord, seen from the leading edge. For the sensitivity analysis, it has been placed at 30% and 50% of the chord, to check the influence. The resulting graphs are shown in figure 3.3.

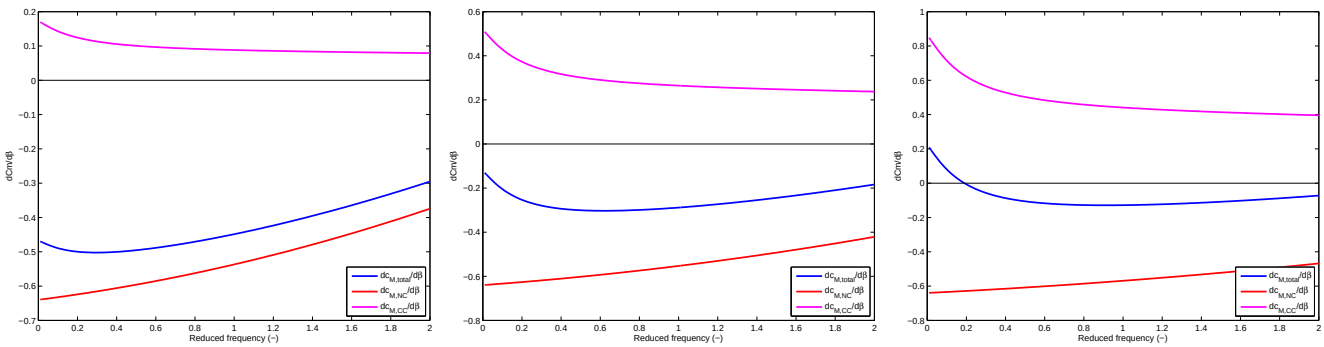

(a) $\partial c_m/\partial\beta$, $a = -0.4$ (b) $\partial c_m/\partial\beta$, $a = -0.2$ (reference) (c) $\partial c_m/\partial\beta$, $a = 0$

Figure 3.3: Influence of the elastic axis location on the moment control derivative

In these figures, it can be seen that the biggest influence for this frequency range is visible in the circulatory contribution. As stated before, the circulatory contribution is dominant in the lift force for low oscillation frequencies and as the moment coefficient depends greatly on the strength of the lift force, it is no surprise that it is also dominant here. It should be noted that the non-circulatory contribution is similar for the stationary case ($k = 0$) in each case, but that it increases quicker as the elastic axis is located closer to the leading edge. In this frequency range, however, this is only of little influence.

Free-stream velocity

The free stream velocity is an important quantity in this analysis, as it sets the limit for which situations this analysis is applicable. For velocities for which the Mach number exceeds 0.3, the incompressibility assumption is no longer valid and hence, there is an upper limit for the free-stream velocity for which this analysis is valid. When considering the used equations, it seems at first sight that V_∞ has some influence, as terms do not directly cancel out when the coefficients are considered, but there is a crux in this story. For example, when considering the term between brackets in the circulatory part of the lift (equation 3.5), it seems like only two out of three terms contain V_∞. However, as β is prescribed and it is known to be harmonic, the frequency appears in front of the harmonic term with power one. The frequency is determined from the reduced frequency according to $\omega = \frac{kV_\infty}{b}$, such that it turns out that $\dot{\beta}$ contains V_∞ and likewise that $\ddot{\beta}$ contains V_∞^2. Knowing this and considering the used equations again, it is observed that for both the lift and the moment, V_∞^2 can be taken out of brackets, which cancels when determining the respective coefficients. Hence, it can be concluded that the free-stream velocity does not influence the control derivatives, something that indeed turned out when consulting the MATLAB model.

Aileron deflection

The maximum aileron deflection in the reference case is 3°, which means that the aileron oscillates harmonically with ±3° with respect to the airfoil. In the model, this oscillation amplitude can be modified to any physically possible

angle, but it should be noted that the theory used has been derived for *small* angles only and hence, only relatively small angles can be considered. When consulting the model, it turns out that the maximum aileron deflection has no influence at all on the control derivatives. This makes sense when considering the used formulas, in which the force and moment increase as β increases, but as the derivative of the coefficients with respect to β is taken, nothing changes as β changes according to the same behaviour. Of course, the coefficients themselves do change as the peaks in lift generation increase with increasing peaks in β, as shown in figure 3.4. It should be noted here that hte phase delay remains constant.

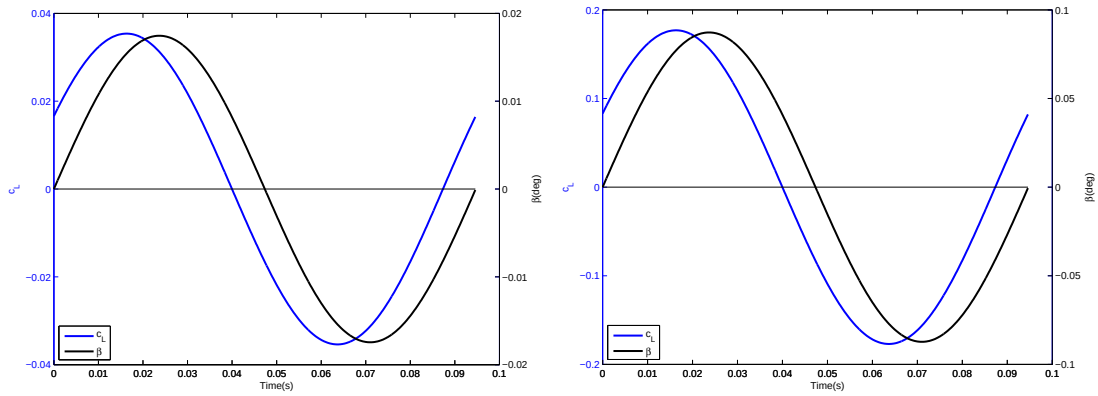

(a) $\beta_0 = 1°$ (b) $\beta_0 = 5°$

Figure 3.4: The progress of c_l in time for different values of β_0, using $k = 1$

Angle of attack

The angle of attack itself changes nothing to the original figures of the control derivatives as function of the reduced frequency, it only changes the equilibrium line of the coefficients. As shown before, with no aileron deflection the lift coefficient is given by the flat plate lift theory using $\partial c_l/\partial\alpha = 2\pi$, such that $c_{l,k=0} = 2\pi\alpha$.

Aileron location

Probably the most interesting variation is to check the influence of the aileron geometry. In the reference situation the aileron consumed the last 20% of the airfoil, but in theory it can consume anywhere between the last 0 and 100% of the airfoil. For comparison, the lift control derivative is considered here, as it says something about the effectiveness of the airfoil. The aileron location c is varied between -1 and 1, such that that all physically possible options — though these are not all applicable in practice — are considered. The reduced frequency has to be fixed in this case, such that for several different situations it can be seen what aileron size is the most effective. In figure 3.5 the most effective point is indicated for $k = 0.5$, $k = 1$ and $k = 1.5$. The moment control derivative as a function of the aileron location has also been visualized, the result of this is shown in figure 3.6.

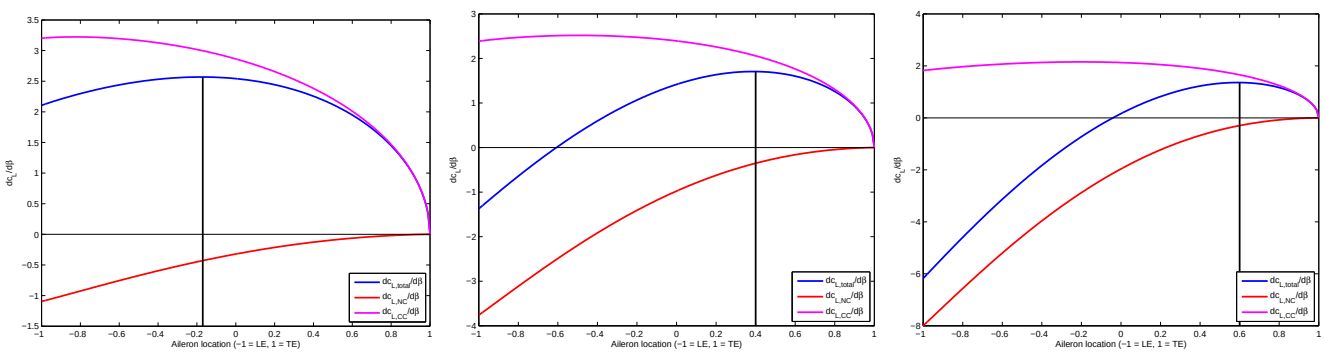

(a) $k = 0.5$ (b) $k = 1$ (c) $k = 1.5$

Figure 3.5: $\partial c_l/\partial\beta$ as a function of the aileron location c

As can be seen, the most effective aileron location moves towards the trailing edge as the reduced frequency increases. In figure 3.6 it can be seen that the difference between the extreme values of the circulatory and non-circulatory contributions grow larger for increasing k. However, when considering the total control derivative in the domain where c is usually applied ($c \in [0.5, 1]$), it can be seen that the differences are small and that the lowest occurring value

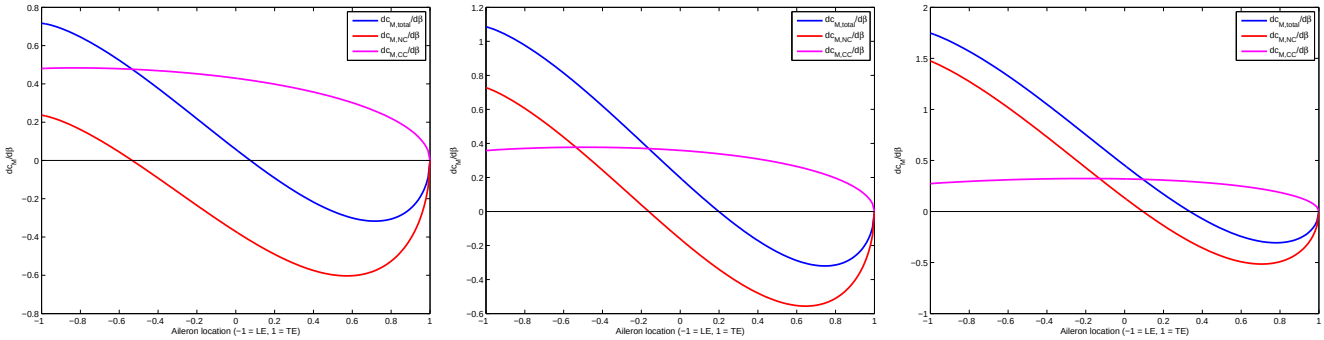

(a) $k = 0.5$ (b) $k = 1$ (c) $k = 1.5$

Figure 3.6: $\partial c_m / \partial \beta$ as a function of the aileron location c

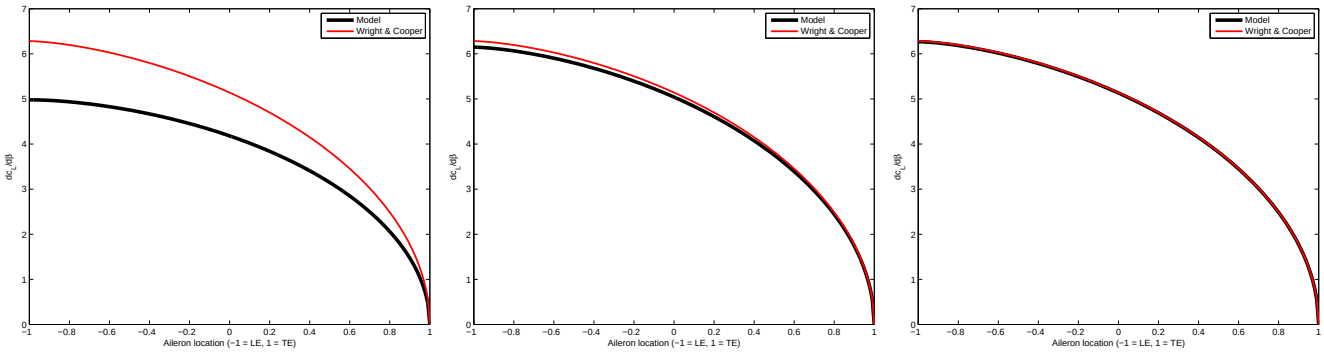

(a) $k = 1 \cdot 10^{-1}$ (b) $k = 1 \cdot 10^{-2}$ (c) $k = 1 \cdot 10^{-3}$

Figure 3.7: $\partial c_l / \partial \beta$ as a function of the aileron location c, determined in two ways.

hardly changes.

The situation of varying c can also be compared with the empircal relations from Wright & Cooper [7], as defined in equation 3.12. As the ratio of chords E is a function of c, this can easily be implemented. Figure 3.7 shows nicely how the values of the lift control derivative as determined by the model approach those determined by equation 3.12 as the reduced frequency asymptotically tends to zero.

4 Numerical model in CFD

4.1 Modeling background

In order to compare results and to investigate the influence of gap flow a similar situation as in the previous chapter has been modeled and analyzed using CFD. Instead of a flat plate, a thin, symmetrical airfoil is used here to prevent difficulties due to singularities which might cause trouble at e.g. the leading and trailing edge. The airfoil used here is the NACA0012, a standard, symmetric and thin airfoil, which makes it suitable for comparison. The solver used for the CFD calculations is SU^2 (Stanford University Unstructured) [8], which is an open-source solver using C++ , initially developed by Stanford University, suitable for solving PDE constrained problems. In order to investigate the influence of gap flow, four different gap situations have been considered, each with a different size.

4.1.1 Meshing

For each different gap size, a different mesh of similar size has been provided. The gap sizes used are 0, 2, 4 and 6% of the flap chord. While the chord of the flap, the control surface, is 20% of the total chord (see table 3.1) this means that the gap sizes are 0, 0.4, 0.8 and 1.2% of the total chord. Normally, such meshes are relatively straightforward, but this case is somewhat more complicated. As the oscillation frequency of the flap is another main parameter of which the influence is desired to be known, the mesh also has to be able to vary in time, as the position of the flap also varies over time. The mesh has been made such that the oscillation parameters (motion origin, oscillation frequency, equilibrium, amplitude) can be set in the configuration file needed for the computation.

In figure 4.1b, the mesh is shown for the situation without a gap and with the flap in the equilibrium position, i.e. the airfoil is fully symmetric. For clarity, the fully meshed domain and a zoomed view of the trailing edge are shown as well. It should be noted that the trailing edge does not have zero thickness, in order to prevent computation singularities like infinite gradients.

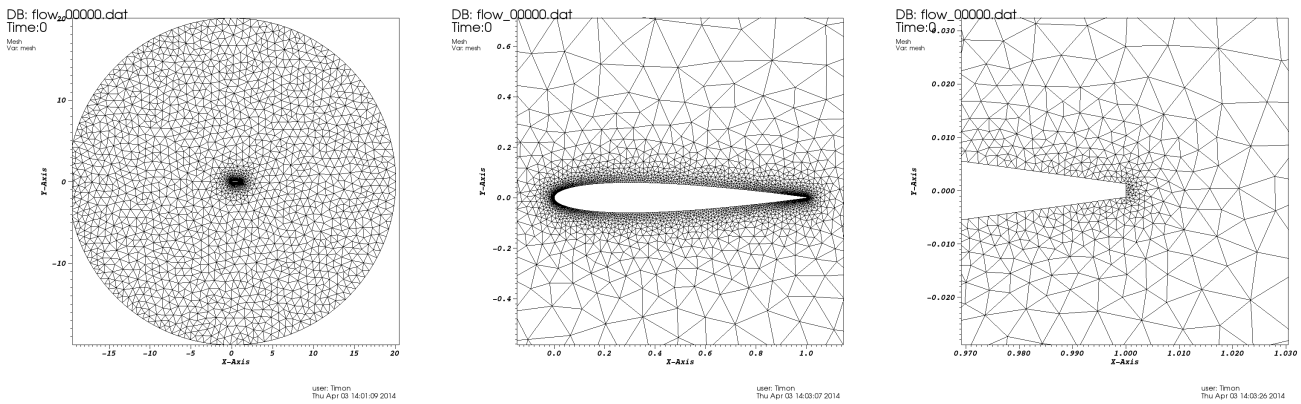

(a) Full view (b) The airfoil (c) Trailing edge

Figure 4.1: The mesh seen from different zoom levels, for the case without gap, no flap deflection.

The flap oscillation is illustrated in figure 4.2. As small perturbations have been assumed, the maximum flap deflection has been taken as 3°. In figure 4.2, the airfoil is shown for the cases of the flap in maximum downward deflection, equilibrium position and maximum upward deflection, respectively.

Like said before, the gap size has been varied as well. In figure 4.3 a zoomed view of the gap is shown for case without gap, the case with a small gap (2% of the flap chord) and for the case with a large gap (6% of the flap chord). It should be noted that the gap is shown here for the situation that the flap is deflected upward maximally.

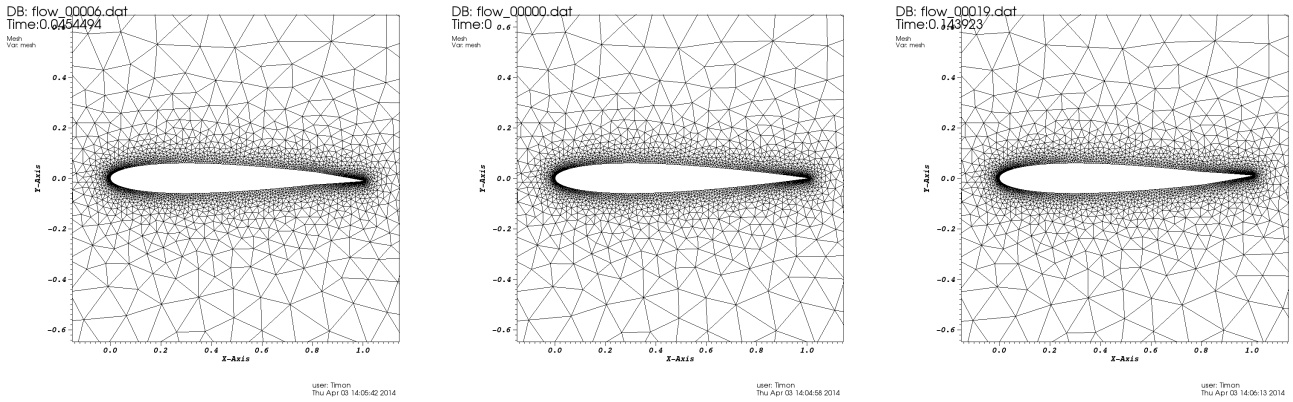

(a) Max. downward deflection (b) Equilibrium position (c) Max. upward deflection

Figure 4.2: The aileron shown in the extreme positions.

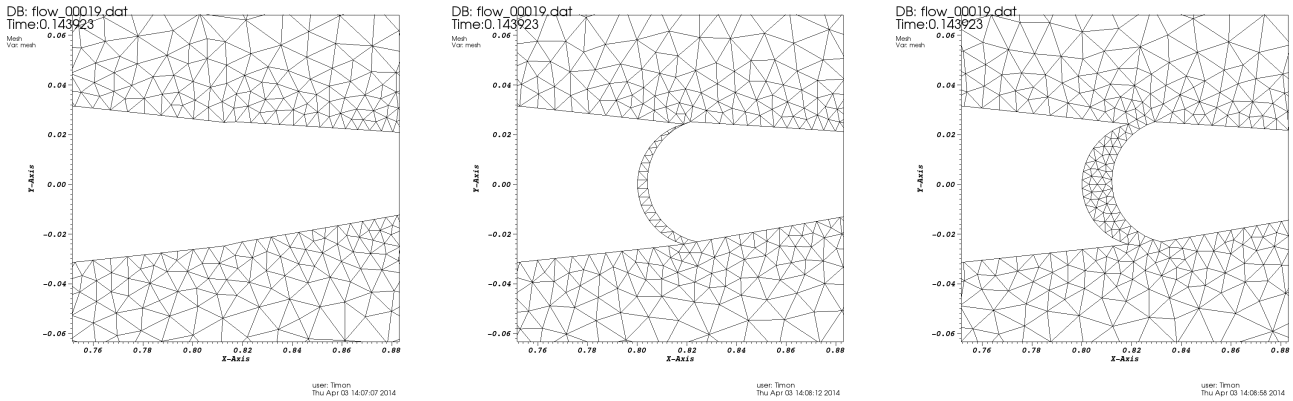

(a) No gap (b) Small gap (c) Large gap

Figure 4.3: Different gap sizes.

4.1.2 Analysis parameters

For each analysis, several parameters have to be set beforehand, in order to specify the flow and computation conditions:

- The flow conditions, such as the Mach number, temperature, pressure, gas constant, γ. For this, the reference case value of $M = 0.2$ has been used, in combination with standard settings for the other parameters, which are also partly shown in table 3.1 for the reference case ($T = 273.15\ K$, $p = 101325\ Pa$, $R = 287.87\ J/kgK$, $\rho = 1.2886\ kg/m^3$ and $\gamma = 1.4$).
- Time step, for a balance between precision and computation time it has been chosen to perform 25 iterations for each period. Such an iteration is later on referred to as a *external iteration*.
- Time domain, in order to get rid of entrance effects four periods have been computed each analysis.
- Oscillation frequency, which can be determined using the reduced frequency and the Mach number.
- Maximum deflection of the oscillating surface, which has been kept to 3°
- Angle of attack, which has been kept at 0°, such that all lift generated comes from the oscillating control surface.

These analysis parameters are all specified in the *configuration file*, which, together with the mesh file, provides all the manual input needed to solve the problem in SU^2.

In addition to the list shown, there is one more parameter to set and this is probably the most important setting to specify in the configuration file. This setting concerns the problem is that is to be solved. There are several options to select from, including some very general ones like the *Navier-Stokes* or *Reynolds Averaged Navier-Stokes* equations. However, as common for a Fluid Dynamics problem these calculations need a lot of time to converge. Due to the available time and the available computation machine it has been chosen to solve the *Euler* equations instead, which drop the viscosity and heat conduction terms in the Navier-Stokes equations and hence provide a useful simplification with a much shorter computation time, but at the cost of accuracy and plausability.

4.2 Performed analyses

In order to check the two core variables of this project, the gap size, here shown as ζ, and the oscillation frequency of the aileron, presented by the reduced frequency k, several analyses have been performed.

For the gap size, all available meshes with differing gap sizes have been analyzed using two different reduced frequencies: $k = 0.2$ and $k = 1$, corresponding with approximately 1.056 Hz and 5.281 Hz, respectively. As four different meshes are available, this equals eight different runs in SU^2.

For the frequency influence, the mesh with a 2% flap chord gap size has been used. Apart from the results for $k = 0.2$ and $k = 1$, which have already been obtained from the first set of analyses, the situations with $k = 0.05$, 0.1, 0.4, 0.6, 0.8, 1.25, 1.5, 1.75 and 2 have also been considered. This roughly corresponds with the domain considered in the theoretical model (see figure 3.1), but more focused on the domain $k \in (0, 1]$, as the biggest differences are expected to occur in that domain.

$k \diagdown \zeta$	0	2	4	6
0.05		•		
0.1		•		
0.2	•	•	•	•
0.4		•		
0.6		•		
0.8		•		
1.0	•	•	•	•
1.25		•		
1.5		•		
1.75		•		
2.0		•		

Table 4.1: The performed analyses

In conclusion, for the influence of the gap size, eight different analyses are needed, the influence of the frequency requires nine more.

4.3 Varying gap size

4.3.1 CFD results

In this section, the progress of c_l for increasing gap size is investigated, hereby leaving the reduced frequency constant. The value for k has been set at both 0.2 and 1 to check if the gap size influence changes for a higher frequency.

$k = 0.2$

In this case, the corresponding frequency is approximately 1.056 Hz, which still means a relatively low frequency. As stated before, the response to the last oscillation period is considered only, in order to neglect any possible entrance effects. The results for the lift and moment coefficients are shown in figure 4.4.

$k = 1$

In this case, the corresponding frequency is five times higher as in the previous case, so it approximately equals 5.281 Hz. Again, the response to the last oscillation period is considered only. The results for the lift and moment coefficients are shown in figure 4.5.

As can be seen, in both cases the results seem to be a bit odd, as one might expect the highest peaks to occur for the case without gap and that the peak amplitude decreases for increasing gap size. The former seems to be the case, the latter does not. This suggests that the modeled airfoils are not symmetrical, but this is not the only possible explanation. This issue will be considered later on in the discussion of the results, in section 5.2.

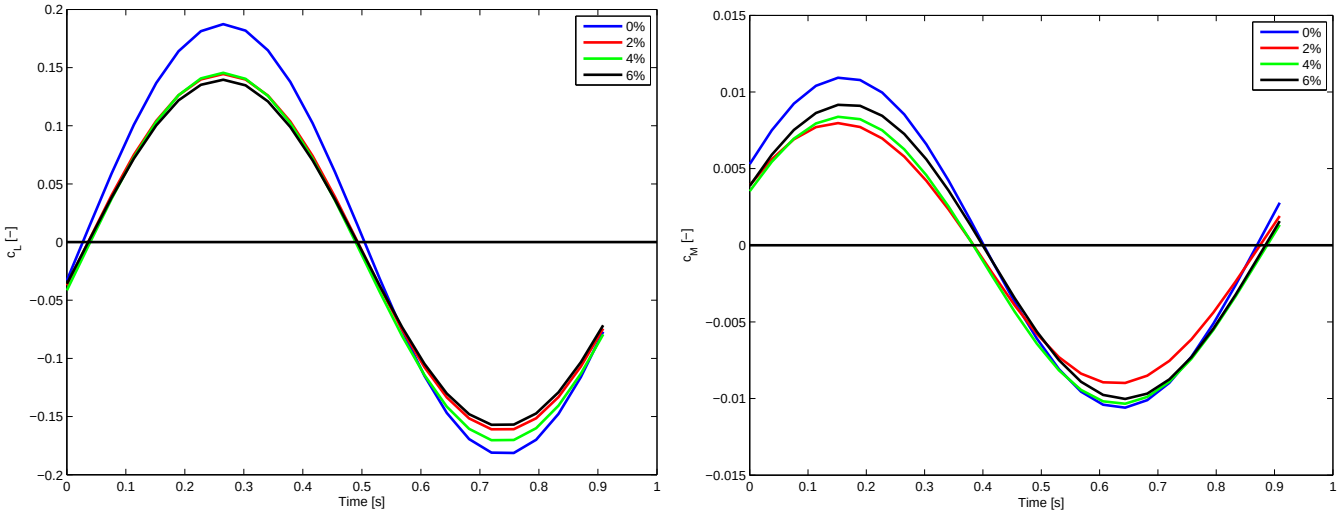

(a) c_l (b) c_m

Figure 4.4: The lift- and momentcoefficient for $k = 0.2$

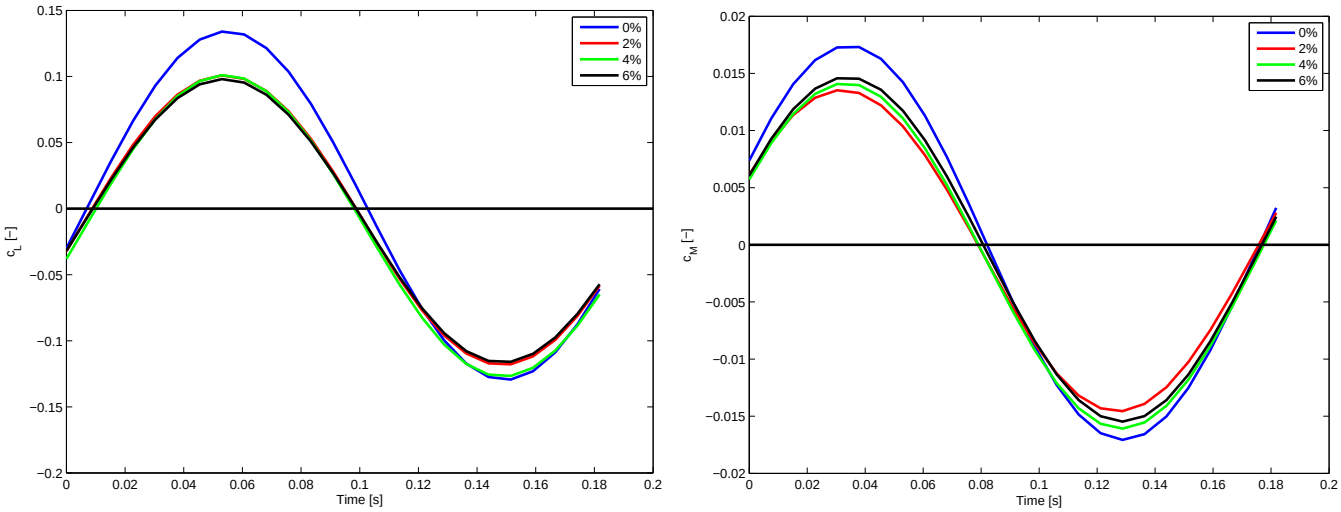

(a) c_l (b) c_m

Figure 4.5: The lift- and momentcoefficient for $k = 1$

4.3.2 Comparison with potential theory

In the broad scope of the project, the goal is to set up a procedure to produce correction functions for the control derivatives when going from theory to practice — where in this project the practical situation is represented by CFD. This means that the values of $\partial c_l/\partial\beta$ and $\partial c_m/\partial\beta$ obtained from the CFD are to be compared with the value obtained from the MATLAB model. However, because of the way these derivatives are computed from either the potential flow model or from CFD, the $\partial\beta$ part is the same, and hence, only the coefficient itself has to be considered instead of its derivative. One way to do this is to take an FFT (Fast Fourier Transform) of the coefficients and extract the highest amplitude, which occurs at the oscillation frequency. Dividing these amplitudes with the amplitude of the respective coefficients obtained from the potential theory model yields the same result as when dividing the control derivatives. This is due to the fact that, as mentioned before, the $\partial\beta$ term is similar (numerically) and because both responses are harmonic. Doing so for both coefficients and plotting this as a function of gap size yields the result shown in figures 4.6a and 4.6b for $k = 0.2$ and $k = 1$, respectively.

As can be seen, the results have been presented as a data plot and with a function fit. This function fit represents the function $F(\zeta)$, where ζ is the gap size as a percentage of the aileron chord, which gives the correction factor for the control derivatives for every ζ. As only a few points are available, a polynomial of third order is the most accurate possible function fit that can be made. It would have been desirable to construct these figures using more data points, but as each extra data point means a change in geometry and therefore a new mesh, only four different points are considered here.

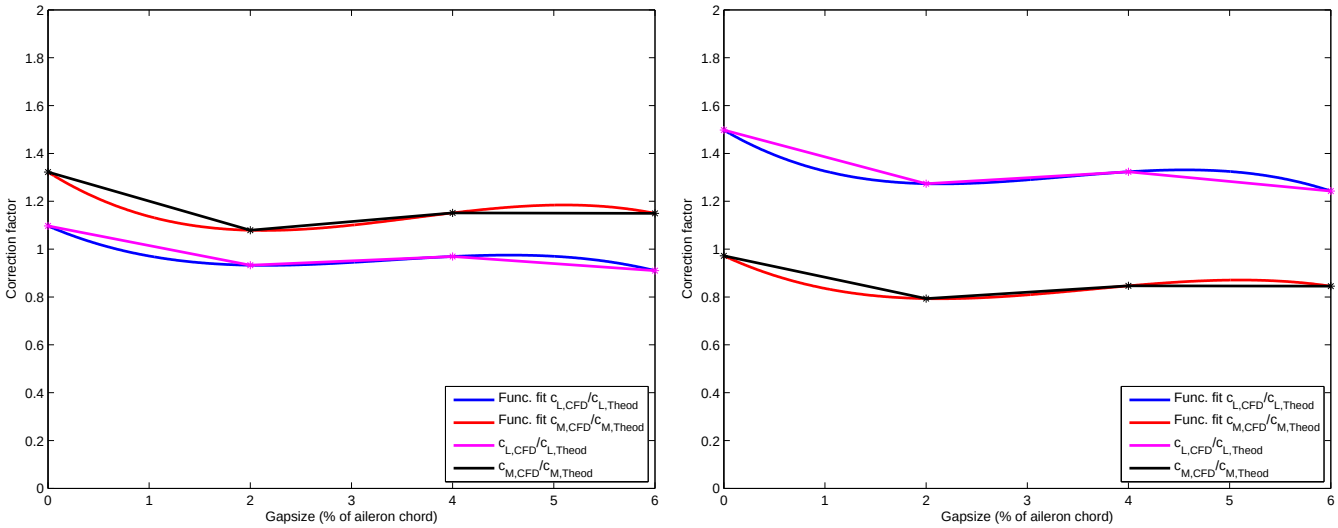

(a) For $k = 0.2$

(b) For $k = 1$

Figure 4.6: Correction functions for the lift- and moment coefficient

What, however, does draw ones attention is that the lines for the correction factor shown in figure 4.6 do not show any type of regression with increasing gap size, as would be expected. As each value is compared with the same value from the potential theory — gap size is the only variable here and this variable plays no role in the used potential flow theory — one would expect some kind of regression with increasing gap size. This does not seem to be the case and highly questions the result. Because of this, some more attention will be given to this topic in the discussion of the results (section 5.2).

It should also be noted that the difference between the correction factors between the two investigated cases ($k = 0.2$ and $k = 1$) is quite significant. This is definitely something to consider in further studies, as will also be mentioned in the recommendations (section 5.3).

4.3.3 Gap flow observations

The flow in the proximity of the gap is interesting to examine, especially when considering the validity of the model. One way to more closely look at this is by considering the pressure coefficient distribution over the airfoil. In figure 4.7a this distribution is shown. For clarity, the y-axis has been reversed such that the top line represents the upper surface of the airfoil. Furthermore, the data for the airfoil and the control surface have been separated for clarity. Also the volume flow solution containing the local velocity has been included, this can be seen in figure 4.7b.

From the right figure in 4.7, it can be seen that within the gap the velocity is almost zero. However, the discontinuity in the surface due to the presence of the gap leads to a large reduction in the flow velocity over the remainder of the airfoil, the majority of which consists of the control surface. As this is the only part of the airfoil to generate lift, this significantly reduces the amount of lift produced. As this does not happen in the case without gap, this might possibly explain the big difference between the gap and no-gap results.

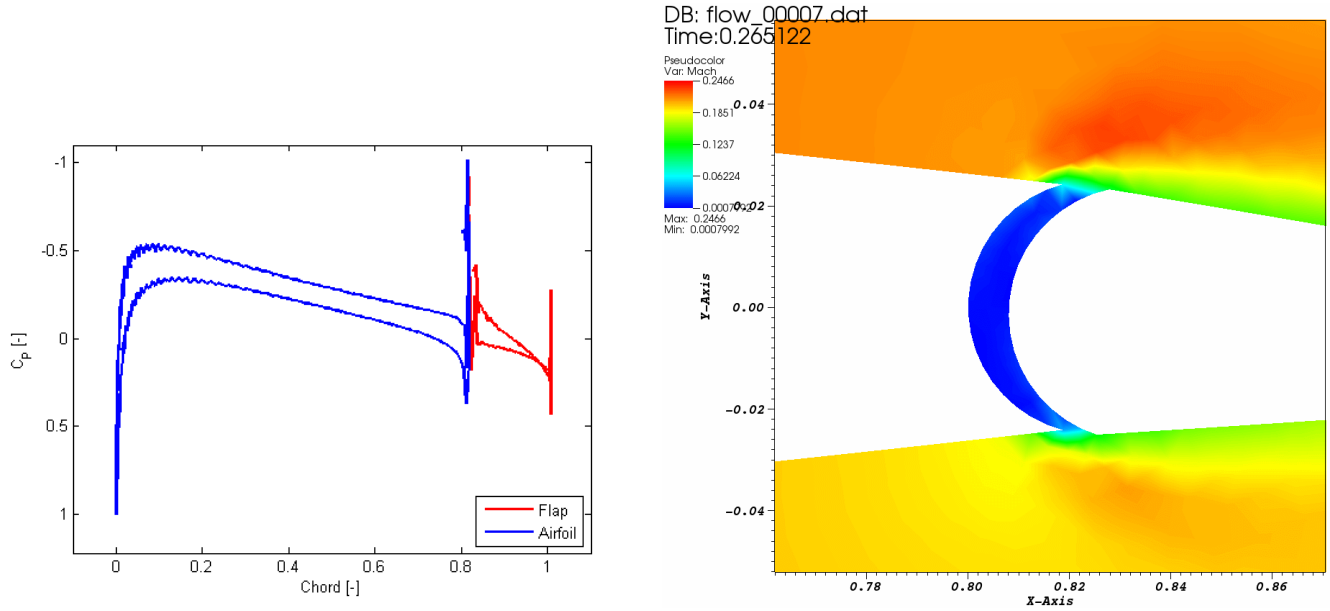

(a) Surface solution (C_p)

(b) Flow solution (M)

Figure 4.7: Distribution of C_p over and of M around the airfoil, for a 4% flap chord gap with maximum downward flap deflection.

4.4 Varying frequency

Another main goal of this research is to reconstruct figure 3.1 using CFD, in order to be able to set up a correction function $F(k)$ in the shape of:

$$\left(\frac{\partial c_l}{\partial \beta}\right)_{real} = F(k) \cdot \left(\frac{\partial c_l}{\partial \beta}\right)_{theory} \tag{4.1}$$

For this, it is necessary to use a single mesh to perform several analyses, using varying values for the reduced frequency. In the reference case results (as presented in figure 3.1), the domain for the reduced frequency is $k \in [0, 2]$, but most changes take place in the case of the lower frequencies. Therefore, it has been chosen to perform more analyses on the domain $k \in [0, 1]$. In total, analyses have been performed for $k = 0.05$, 0.1, 0.2, 0.4, 0.6, 0.8, 1, 1.25, 1.5, 1.75 and 2 in order to get a reasonable representation for the CFD results for the control derivatives as a function of k. More data points would provide a greater accuracy, but for every data point another analysis is needed, which, as stated before, is costly.

4.4.1 CFD results

The results of these analyses are shown in the figures in 4.8. For clarity, the theoretical result from the potential flow theory has been included in the figure.

Contrary to the case of varying ζ, the CFD results show logical behaviour, especially when compared with the potential theory results. The observant reader might have noticed that the line showing the result from potential theory differs from the one presented in figure 3.1. This is due to the fact that in figure 3.1 only the real part is shown, whereas figures 4.8a and 4.8b show the absolute values. While this may sound somewhat odd, the former has been done to be able to properly split the circulatory and non-circulatory parts of the flow. As these results were only meant to distinguish between the two flow contributions, this is not necessary in this case and hence, it is logical to display the more correct absolute value here.

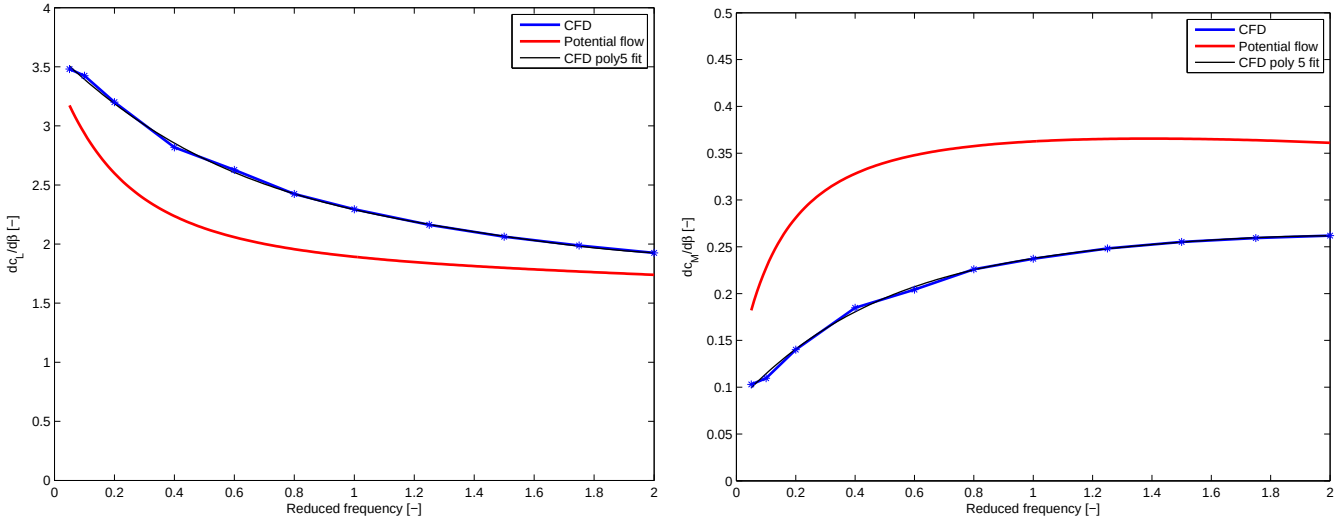

(a) c_l (b) c_m

Figure 4.8: Correction factors for the lift- and moment coefficient

4.4.2 Correction functions

As can be seen in figures 4.8a and 4.8b a function fit with a 5th degree polynomial has been applied to the data points for the CFD results. This way the result can be interpolated between the data points to get a relatively accurate prediction of the control derivatives on the domain $k \in [0.05, 2]$. Using this function fit, the value of the control derivative can be divided with the potential flow result for each incremental step in k. This results in a vector on the specified domain for k with a value at each increment. Again, a polynomial fit can be used, this time to estimate a function $F(k)$ on the domain $k \in [0.05, 2]$. In figure 4.9 the correction factor is shown as a function of k, using the data points and using a 6th degree polynomial through these data points.

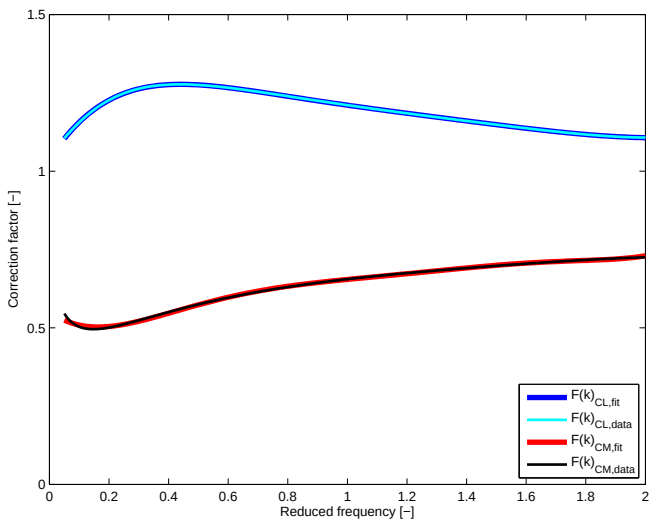

Figure 4.9: Correction functions for both control derivatives

In this figure, it should be noted that the correction factor for $\partial c_l/\partial\beta$ does not differ that much over the domain, but that the potential theory results predict and underestimation of this control derivative. Remarkably, the difference between the results is the largest around $k = 0.4$, close to the point where the phase delay of the Theodorsen function is maximal.

The correction function $F(k)$ that is sought for is here only presented as a visual result in the graph. Providing the coefficients of the polynomial as a result is not directly relevant here as this is only a test case which was needed to verify that the model is indeed functioning correctly.

5 Conclusions and Recommendations

The main conclusion that can be drawn from the obtained results is that it is possible to define a procedure that determines correction factors for the lift and moment coefficient derivatives as a function of the reduced frequency and the gap size, but not without making some serious remarks about the obtained results. The section below describes briefly how these correction functions have been obtained during this research, then discusses the plausability and limitations of the results and finally gives some recommendations about this work and possible future works.

5.1 General procedure

First of all, the necessary theoretical background based on potential theory as explained by Theodorsen has been described. This theory has been the basis for the theoretical model presented in section 3.2, which is valid for:

- Unsteady flow
- Incompressible flows (low velocities)
- Inviscid flow
- Irrotational flow
- Conservative force field

Afterwards, this theory has been extended to include the effects of an oscillating aileron. Finally, the Kutta condition has been applied to enforce flow separation at the trailing edge. Doing so, the force and moment can be determined and using those, the corresponding dimensionless coefficients and their derivatives. The programmed model in MATLAB separately calculates the circulatory and non-circulatory parts of the lift and moment contribution in order to see for which aileron oscillation frequencies what contribution has the most influence. It turned out that for low frequencies the circulatory part of the flow is dominant, while for higher frequencies the non-circulatory part is dominant. This is due to the amplitude of the deflection angle derivatives which appear in the terms of the respective contributions for the control derivatives. A sensitivity analysis on this model showed that for each frequency, the aileron has an optimal size for the lift efficiency of the airfoil, ranging from 60% in case $k = 0.5$ to 20% in case $k = 1.5$. It should be noted that these values are not necessarily values that reflect a possible application in practice, but they have solely been presented as the result of a theoretical model. The model has been validated using Cooper's empirical relation for zero oscillations. Finally, a correction factor between the potential theory and Cooper's relation has been determined and visualized. As expected, this factor is 1 for $k = 0$ and smaller than 1 for $k > 0$, for both control derivatives.

The scope of the project was to define a procedure that determines the functions $F(k)$ and $F(\zeta)$ that give a correction factor for the control derivatives as a function of the reduced frequency k and gap size ζ, respectively. In this way, real-life values for the control derivatives can be estimated using the relatively simple potential theory and these functions. In order to achieve this, CFD analyses have been run using a symmetric airfoil which simulates the real-life results. The results have been analyzed using MATLAB and using a sixth and a third order polynomial function fit, the functions $F(k)$ and $F(\zeta)$ have been determined, respectively.

This means that, assuming that enough experimental or CFD data for a specific wing type have been obtained, the functions $F(k)$ and $F(\zeta)$ can be defined and used for in-flight applications. According to the sensitivity analysis for the theoretical model carried out in chapter 3.3 any applicable flight parameter may be altered without changing the coefficients of the specified correction functions, but a similar sensitivity analysis for the CFD results still lacks. A possible application for these correction functions might be to predict, while in-flight and using the flight conditions of that moment, the reaction of the aircraft to the oscillation of the aileron using only the potential theory outlined here and the defined correction functions.

5.2 Discussion

While considering the obtained results throughout this report, it has been mentioned several times that these are somewhat questionable. In this section, the plausability and correctness of the obtained results is considered in order to define what more is necessary to consider in future works.

5.2.1 Validity of the model

Incompressibility assumption

One of the main assumptions of this analysis is that the flow is incompressible. As stated before, a Mach number of lower than approximately 0.3 is needed to ensure that the deviation of the density is still within limits. In the reference case it has been chosen to use $M = 0.2$ in order to be significantly lower than this limit, but as the flow over the wing accelerates, Mach numbers higher than 0.2 will be present in the flow. In order to check if these do not exceed the limit value of 0.3, the Mach number in the flow has been visualized in VisIt. As the lift coefficient is the highest for the case without gap, it is important to check what the highest occurring Mach number is in this case. In figure 5.1 the Mach number distribution around the airfoil is shown, for the case of the highest occurring Mach number. This turns out to be so when the aileron is deflected downward maximally, the corresponding maximum Mach number turns out to be lower than 0.25. Considering this, it is valid to state that the incompressibility assumption holds.

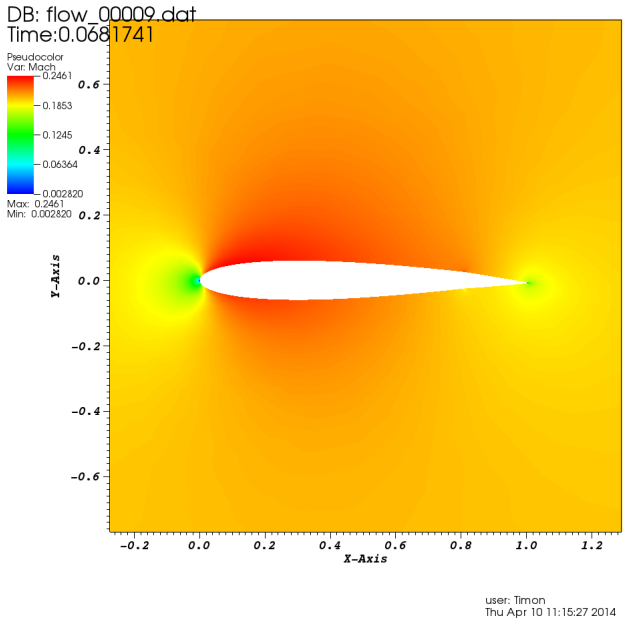

Figure 5.1: Mach number distribution around the airfoil for zero gap, $k = 1$ and maximum downward aileron deflection.

Flow separation

Another phenomenon to be checked is flow separation at the trailing edge. In the potential theory, the Kutta condition is applied to ensure this. In the CFD analyses, it can manually be checked whether flow separation occurs or not. If not, the flow is physically not possible and the obtained results should be reconsidered.

In order to check the flow separation, a contour plot of the velocity has been made, zoomed in at the trailing edge. This figure is shown in figure 5.2. As can be seen, the contours close to the airfoil surface at the trailing edge can be considered parallel to the airfoil surface, showing that flow separation indeed occurs.

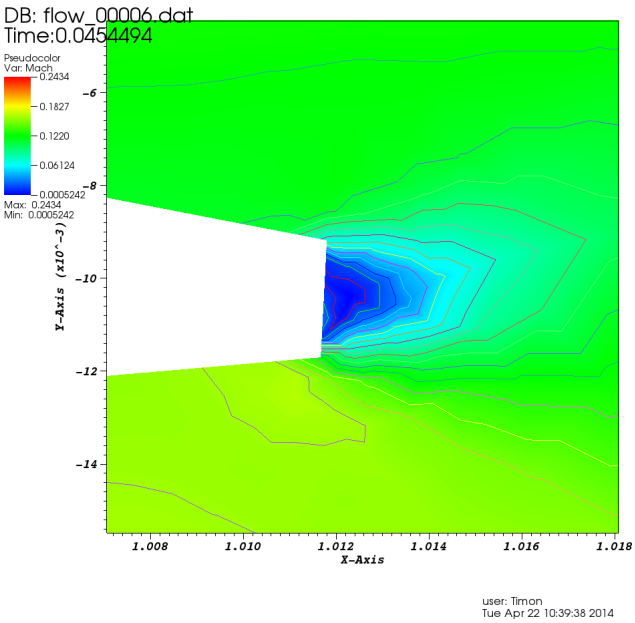

Figure 5.2: Mach number distribution around the trailing edge with $k = 1$ and maximum downward aileron deflection.

5.2.2 Limitations of the used theory

The model produced in MATLAB is based on the Theodorsen potential theory, which imposes several limitations. The biggest limitation in the application comes from the incompressibility assumption, which limits the maximum Mach number for which the model is applicable to 0.3. If it would be desired to consider higher velocities as well, the compressibility correction could be used to account for this. However, higher velocities have other downsides, which might effect the inviscid flow assumption that this model contains. Viscous effects like boundary layer effects start playing a large role for higher velocities and need a different approach.

Furthermore, the airfoil used in the potential theory is a flat plate, which is symmetric. In the CFD calculations it has been compared with a NACA0012 airfoil, which does have a thickness, but still no camber. In this way, effects caused by the asymmetry of an airfoil are eliminated. In case airfoils with a significant camber are applied to this procedure, it should be kept in mind that effects caused by the asymmetry may start playing a role.

The theory directly assumes a two-dimensional situation and therefore neglects any three-dimensional effects. Wings generally have no constant profile and chord, which is not accounted for here. Leakage flow around the wing tips that reduce the pressure difference and therefore the amount of lift generated — while using the same ambient conditions — could be accounted for using induced-drag theory, but this has not been included in this model.

5.2.3 Discussion of the CFD results

The CFD results that have been obtained show some oddities, which will briefly be described here. First of all, as was already observed in figures 4.4 and 4.5, the results appear to be asymmetrical. This has been more closely examined by repeating the calculations, but only using a very small value for β_0. In the reference case, the maximum excitation of the aileron was 3°, while in the repeated case only 0.1° has been used. The result of this calculation is shown in figure 5.3, which indeed shows some asymmetry.

For the calculations themselves, this asymmetry is not a significant problem, as only the amplitude of the oscillation is important and not its equilibrium position. However, as the airfoils and the corresponding meshes have been designed to be symmetrical, this does indicate that there is another problem causing this asymmetry. This can either be anything from a numerical calculation problem to a meshing problem, but time prevents us from closely examining this.

Another problem, as mentioned in the previous chapter, is that the correction factors shown in figure 4.6 do not show a logical regression. In order to consider this somewhat further, figure 4.4a has been reproduced but in order to better compare the lines, each line has been adjusted such that the average value is zero. This result is shown in figure 5.4.

As can be seen, the peak values indeed seem to be in the wrong order, as the lift coefficient in case of the 2% gap is expected to show higher peaks than the one with the 4% gap, which is not the case. This is not realistic and should

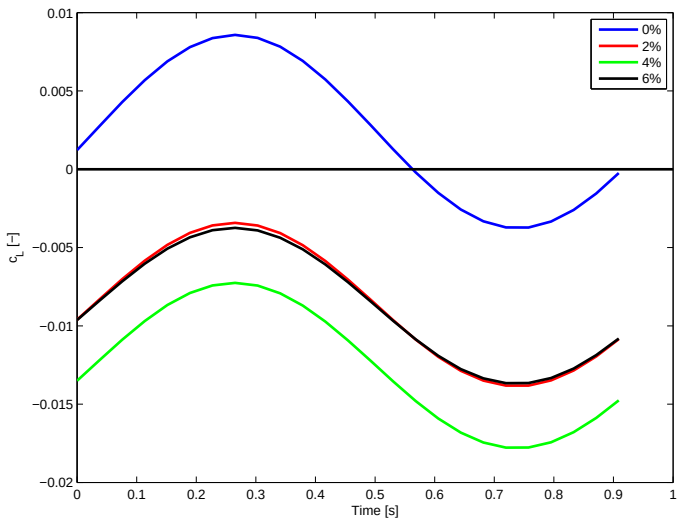

Figure 5.3: c_l for $k = 0.2$ and $\beta_0 = 0.1°$

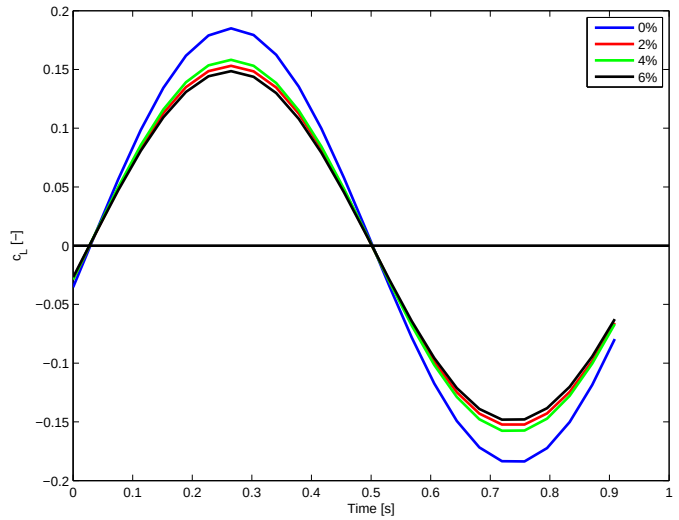

Figure 5.4: c_l for $k = 0.2$, $\beta_0 = 3°$ and corrected for asymmetry.

definitely be considered more thoroughly before continuing any research.

A possible cause of these problems might be that the used mesh is not a very fine one, introducing some more error. The amount of elements was fairly low to obtain the necessary results more quickly and to be able to use a smaller machine. Refining the computational grid near the airfoil, especially near the gap and the trailing edge would result in more precise results, but inevitably also at a higher cost. The movement of the mesh due to the oscillating aileron has not been considered as risky here, but it could impose other problems. Altering the geometry causes elements to get a different aspect ratio, which might eventually lead to a mesh that is not fully converged. Before running future simulations, the mesh for every time step should be considered carefully to avoid such problems.

5.3 Recommendations

As described before, this project has only outlined the general procedure of correcting the control derivatives as a function of the reduced frequency and gap size, but using questionable data to simulate a real-life situation. In order to make this whole procedure more accurate and plausible, some recommendations have been done for possible future works:

- The plausibility of the procedure as a whole can be increased if the analysis "grid" as shown in table 4.1 would be refined, expanded and performed fully using either wind tunnel tests or more accurate CFD runs.
- For further applications using CFD, a proper balance between accuracy and cost should be made. In this case, the computational cost has been very low, but the accuracy is highly questionable. Meshes that produce results that show less oddities are desired if this procedure is to be applied in a real life situation.

- The mesh movement should be considered more carefully to check if this produces other problems that have not yet been considered. Ideally, the CFD results should be compared to experimental results in order to check this.
- The CFD cases should be subjected to an extensive sensitivity analysis, like has been done for the potential flow model. As this costs quite a lot of computation time this has been ignored in this project, but this will provide some very useful insight in the applicability of the model in general.
- Gap flow, which did not appear in the results produced here but which would surely appear in experimental results, has only been considered briefly but should be investigated more thoroughly. In the grid shown in table 4.1 way more gap sizes should be considered to be able to more accurately look for gap size dependencies.
- In the theoretical model the gap flow was not considered. Some more investigations about the theory behind gap flow should be done in order to be able to include this in the theoretical model. This will give some useful insight about the expected behaviour of the control derivatives and will yield a more accurate correction factor.

List of symbols

Latin symbols

Symbol	Units	Description
a	$[-]$	Elastic axis location
b	m	Airfoil semi-chord
c	$[-]$	Aileron location
$C(k)$	$[-]$	Theodorsen function
C_p	$[-]$	Pressure coefficient
c_l	$[-]$	Lift coefficient per unit span
c_m	$[-]$	Moment coefficient per unit span
E	$[-]$	Ratio of control surface chord and airfoil chord
$F(\zeta)$	$[-]$	Control derivative correction function for gap size
$F(k)$	$[-]$	Control derivative correction function for reduced frequency
F_{NC}	N	Force by non-circulatory flow
F_Γ	N	Force by circulatory flow
h	m	Heave
$\dot{h}$	m/s	Rate of change of the heave
$\ddot{h}$	m/s^2	Acceleration of the heave
k	$[-]$	Reduced frequency
l	N/m	Lift per unit span
m	Nm/m	Moment per unit span
M	$[-]$	Mach number
M_{NC}	Nm	Moment by non-circulatory flow
M_Γ	Nm	Moment by circulatory flow
p	Pa	Pressure
R	J/kgK	Gas constant
T	K	Temperature
V and V_∞	m/s	Free-stream velocity

Greek symbols

Symbol	Units	Description
α	$[-]$	Angle of attack of the airfoil
$\dot{\alpha}$	$[1/s]$	Rate of change of the angle of attack
$\ddot{\alpha}$	$[1/s^2]$	Acceleration of the angle of attack
β	$[-]$	Angle of aileron with respect to the airfoil
$\dot{\beta}$	$[1/s]$	Rate of change of the angle of the aileron
$\ddot{\beta}$	$[1/s^2]$	Acceleration of the angle of the aileron
γ	$[-]$	Infinitesimal circulation (chapter 2)
γ	$[-]$	Gas parameter (chapter 3 and 4)
Γ	$[Nm^2/s]$	Circulation
ε	$[m^2/ms]$	Source strength per unit length
ζ	$[-]$	Gap size between airfoil and aileron
η	$[-]$	Joukowsky transformation coordinate
ξ	$[-]$	Joukowsky transformation coordinate
ρ	$[kg/m^3]$	Density per unit span
ϕ	$[m^2/ms]$	Infinitesimal velocity potential
Φ	$[m^2/s]$	Velocity potential
ω	$[rad/s]$	Frequency

Bibliography

[1] Silvestre, F.J., "Methodology for Modelling the Dynamics of Flexible, High-Aspect-Ratio Aircraft in the Time Domain for Aeroservoelastic Investigations", ISBN: 978-3-86387-316-5, Berlin, Germany, 2013

[2] Theodorsen, T., "General Theory of Aerodynamic Instability and the Mechanism of Flutter", NACA TR 496, 1935

[3] Sadraey, M.H., "Aircraft Design: A Systems Engineering Approach", ISBN: 978-1-119-95340-1, 1st edition, 2012

[4] Nam C., Kim, Y. and Weisshaar, T.A., "Computational Aids in Aeroservoelastic Analysis Using MATLAB^{TM}", 2001

[5] Krzysiak, A., Narkiewicz, J., "Aerodynamic Loads on Airfoil with Trailing-Edge Flap Pitching with Different Frequencies", Warsaw, Poland, *Journal of Aircraft*, Vol. 43, No. 2, 2006, p. 407-418

[6] Liggett, N., Smith, M.J., "The physics of modeling unsteady flaps with gaps", Atlanta, USA, *Journal of Fluids and Structures*, Vol. 38, 2013, p. 255-272

[7] Wright, J. R. and Cooper, J. E.: "Introduction to Aircraft Aeroelasticity and Loads", John Wiley & Sons Ltd, Chichester, West Sussex, UK, 2008, ISBN 0-470-85840-0

[8] F. Palacios, M. R. Colonno, A. C. Aranake, A. Campos, S. R. Copeland, T. D. Economon, A. K. Lonkar, T. W. Lukaczyk, T. W. R. Taylor, and J. J. Alonso, "Stanford University Unstructured (SU2): An open-source integrated computational environment for multi-physics simulation and design", AIAA Paper 2013-0287, 51st AIAA Aerospace Sciences Meeting and Exhibit. January 7th - 10th, 2013. Grapevine, Texas, USA.